MissNODAG: Differentiable Learning of Cyclic Causal Graphs from Incomplete Data

Anonymous authors
Paper under double-blind review

Abstract

Causal discovery in real-world systems, such as biological networks, is often complicated by feedback loops and incomplete data. Standard algorithms, which assume acyclic structures or fully observed data, struggle with these challenges. To address this gap, we propose MissNODAG, a differentiable framework for learning both the underlying cyclic causal graph and the missingness mechanism from partially observed data, including data *missing not at random*. Our framework integrates an additive noise model with an expectation-maximization procedure, alternating between imputing missing values and optimizing the observed data likelihood, to uncover both the cyclic structures and the missingness mechanism. We demonstrate the effectiveness of MissNODAG through synthetic experiments and an application to real-world gene perturbation data.

1 Introduction

Causal discovery, the process of identifying causal relationships from data, is fundamental across scientific domains such as biology, economics, and medicine (Spirtes et al., 2000; Sachs et al., 2005; Zhang et al., 2013; Segal et al., 2005; Imbens & Rubin, 2015). Understanding these relationships is crucial for predicting how systems respond to interventions, enabling informed decision-making in complex systems (Solus et al., 2017; Sulik et al., 2017; Sethuraman et al., 2023). Traditionally, causal relationships are modeled using *directed graphs*, where nodes represent variables, and directed edges encode cause-effect relationships.

Existing causal discovery methods are typically divided into two main categories: *constraint-based* and *score-based* approaches. Constraint-based methods, such as the PC algorithm (Spirtes et al., 2000; Triantafillou & Tsamardinos, 2015; Heinze-Deml et al., 2018), infer the causal structure by enforcing conditional independencies observed in the data, though they often struggle with scalability due to the large number of required conditional independence tests. Score-based methods, such as the GES algorithm (Meek, 1997; Hauser & Bühlmann, 2012), optimize a penalized score function, like the Bayesian Information Criterion, over the space of candidate graphs, usually employing greedy search techniques. There also exist *hybrid* methods which combine elements of both approaches, leveraging conditional independence tests alongside score optimization (Tsamardinos et al., 2006; Solus et al., 2017; Wang et al., 2017). Recent advances have introduced *differentiable* discovery methods, such as the NOTEARS algorithm (Zheng et al., 2018), which frames learning of a Directed Acyclic Graph (DAG) as a continuous optimization problem, enabling scalable and efficient solutions via gradient-based methods. Following NOTEARS, several extensions have been developed for learning DAGs under various assumptions in observational settings (Yu et al., 2019; Ng et al., 2020; 2022; Zheng et al., 2020; Lee et al., 2019).

Most causal discovery methods make one or both of the following assumptions: (i) the data is fully observed, and (ii) the underlying graph is acyclic. However, real-world systems often violate these assumptions. Biological systems, such as gene regulatory networks, and socio-economic processes frequently exhibit feedback loops (cycles) (Sachs et al., 2005; Freimer et al., 2022), while missing data is common in practical applications (Getzen et al., 2023). These complexities significantly limit the applicability of standard causal discovery methods.

Missing data mechanisms are classified into three categories: Missing Completely At Random (MCAR), Missing At Random (MAR), and Missing Not At Random (MNAR) (Little & Rubin, 2019). One common approach to dealing with missing data involves discarding incomplete samples or excluding variables with missing data (Carter, 2006; Van den Broeck et al., 2015; Strobl et al., 2018), which might be suitable only in restrictive settings such as MCAR mechanisms while missingness rate is negligible. Otherwise, it leads to performance degradation as the missingness increases. Another common approach is imputation-based methods where the missing data is first imputed before applying causal discovery algorithm on the data. Some notable imputation algorithms include multivariate imputation by chained equations (MICE) (White et al., 2011), MissForest (Stekhoven & Bühlmann, 2012), optimal transport (Muzellec et al., 2020), and a few deep learning based approaches (Li et al., 2019; Luo et al., 2018). However, imputation-based methods typically assume that data are MAR, which can lead to bias when the data are actually MNAR, a common occurrence in practice (Singh, 1997; Wang et al., 2020; Kyono et al., 2021; Gao et al., 2022). Gain & Shpitser (2018) addresses MNAR data by using reweighted observed cases as input to the PC algorithm alongside a weighted correlation matrix. Additionally, Tu et al. (2019) extends the PC algorithm by incorporating corrections to account for both MAR and certain cases of MNAR, while also learning the underlying missingness mechanisms.

Furthermore, while the acyclicity assumption simplifies computations by factorizing joint distributions into conditional densities, many real-world systems feature cyclic relationships (Sachs et al., 2005; Freimer et al., 2022). Several approaches have been developed to relax the acyclicity assumption, allowing for cyclic causal graphs. For example, early work by Richardson (1996) extended the constrained-based framework to account for cycles, and Lacerda et al. (2008) provide an Independent Componenet Analysis (ICA) based causal discovery for linear non-Gaussian cyclic graphs. More recent score-based methods for learning cyclic graphs include (Huetter & Rigollet, 2020; Améndola et al., 2020; Mooij & Heskes, 2013; Drton et al., 2019). Additionally, methods such as those proposed by Hyttinen et al. (2012) and Huetter & Rigollet (2020) focus on learning cyclic graphs from interventional data. Sethuraman et al. (2023) further extended this line of approach to nonlinear cyclic directed graphs, eliminating the need for augmented Lagrangian-based solvers by directly modeling the data likelihood.

Contributions. In this work, we address two major limitations in causal discovery: the inability to handle informative MNAR data and the restriction to acyclic structures. We propose *MissNODAG*, a general framework that extends expectation–maximization (EM)–based causal discovery to cyclic graphs and arbitrary graphically represented MNAR mechanisms. MissNODAG alternates between imputing missing values and maximizing the expected log-likelihood of the observed data, unifying and extending prior approaches such as MissDAG (Gao et al., 2022). Following Sethuraman et al. (2023) and Behrmann et al. (2019), we employ residual normalizing flows to flexibly model data likelihoods in both linear and nonlinear structural equation models. Our framework accommodates MCAR, MAR, and MNAR missingness and can represent any MNAR process that admits a graphical specification. Through synthetic experiments, we show that MissNODAG outperforms state-of-the-art imputation techniques combined with causal learning on partially missing interventional data. Furthermore, we also provide consistency guarantees for exact maximization of the score function.

The paper is organized as follows. In Section 2, we describe the problem setup and outline the modeling assumptions. Section 3 introduces the proposed expectation-maximization-based MissNODAG framework. In Section 4, we validate MissNODAG on various synthetic datasets. Section 5 concludes the paper. All proofs are deferred to the appendix.

2 Problem Setup

A list of notations is provided in Appendix A for the ease of reference.

Structural Causal Model. Let $\mathcal{G} = (X, \mathcal{E})$ denote a possibly cyclic causal graph with a set of vertices $X = (X_1, \ldots, X_K)$, representing a vector of K random variables connected by directed edges $\mathcal{E} \subseteq X \times X$. We assume the following *structural causal model* (SCM), also known as structural equation model (SEM), with additive noise terms to capture the functional relationships between variables in $\mathcal{G}$ (Bollen, 1989; Pearl,

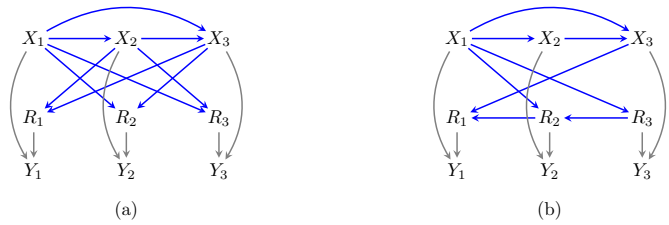

Figure 1: Example m-graphs with three variables illustrating: (a) An example of an MNAR mechanism where no edge of the form $R_i \to R_j$ exists; (b) An MNAR mechanism where R's are connected and the full law is identifiable (no self-censoring and no colluder structures).

2009):

$$X_k = f_k\big(\mathrm{pa}_{\mathcal{G}}(X_k)\big) + \epsilon_k, \quad k = 1, \ldots, K, \tag{1}$$

where $\mathrm{pa}_{\mathcal{G}}(X_k) = \{X_\ell \in X \mid X_\ell \to X_k \in \mathcal{E}\}$ denotes the parents of X_k in $\mathcal{G}$. The function f_k describes the relationship between X_k and its parents, with ϵ_k as the exogenous noise term, assumed to be mutually independent (no unmeasured confounders), and collected as $\epsilon = (\epsilon_1, \ldots, \epsilon_K)$. We assume that self-loops (edges of the form $X_k \to X_k$) are absent in $\mathcal{G}(X)$, as this could lead to model identifiability issues (Hyttinen et al., 2012).

Let $\mathrm{F}(X)$ collect the functions $f_k(\mathrm{pa}_{\mathcal{G}}(X_k))$, for all k. The structural equations in equation 1 can be written as follows:

$$X = \mathrm{F}(X) + \epsilon. \tag{2}$$

Let id denote the identity map, so $(\mathrm{id} - \mathrm{F})$ maps X to ϵ. We assume that this mapping is bijective, ensuring the existence of $(\mathrm{id} - \mathrm{F})^{-1}$, and that both $(\mathrm{id} - \mathrm{F})$ and $(\mathrm{id} - \mathrm{F})^{-1}$ are differentiable. The former ensures that there is a unique X for a given ϵ, thus, we can express X as $X = (\mathrm{id} - \mathrm{F})^{-1}(\epsilon)$. This assumption is needed for our developments in Section 3.3, and is naturally satisfied when the underlying graph is acyclic (Mooij & Heskes, 2013; Sethuraman et al., 2023).

Intervention operations can be readily incorporated into equation 2. In this work, we focus exclusively on surgical, or hard, interventions (Spirtes et al., 2000; Pearl, 2009). Graphically, a hard intervention corresponds to removing all incoming edges to the intervened variable. Following similar notational convention in (Hyttinen et al., 2012; Sethuraman et al., 2023), given a set of interventional targets $X_{\mathcal{I}}$, we can decompose X into disjoint sets, $X = X_{\mathcal{I}} \cup X_{\mathcal{O}}$, where $X_{\mathcal{I}}$ represents the set of intervened variables in an interventional experiment, and $X_{\mathcal{O}}$ represents the set of purely observed variables. We denote the graph obtained after performing the interventions on $X_{\mathcal{I}}$ as $\mathrm{do}(\mathcal{I})(\mathcal{G})$. Let $\mathbf{D} \in \{0,1\}^{K \times K}$ be a diagonal matrix where $D_{kk} = 1$ if $X_k \in X_{\mathcal{O}}$, and 0 otherwise. Under this setting, the SEM in equation 2 is now modified to:

$$X = \mathbf{D}\mathrm{F}(X) + \mathbf{D}\epsilon + C, \tag{3}$$

where C denotes a vector of size K representing intervention assignments for variables in X. Specifically, $C_k = X_k$ if $X_k \in X_{\mathcal{I}}$, and $C_k = 0$ otherwise. Let $\epsilon_{\mathcal{O}}$ denote the exogenous noise terms corresponding to variables in $X_{\mathcal{O}}$. Let $p_{\epsilon_{\mathcal{O}}}(\epsilon_{\mathcal{O}})$ and $p_{X_{\mathcal{I}}}(X_{\mathcal{I}})$ be the joint probability densities of $\epsilon_{\mathcal{O}}$ and $X_{\mathcal{I}}$, respectively. We thus have,

$$p_X(X) = p_{X_{\mathcal{I}}}(X_{\mathcal{I}})\; p_{\epsilon_{\mathcal{O}}}\big(\epsilon_{\mathcal{O}}\big)\; \big|\det J_{(\mathrm{id}-\mathbf{D}\mathrm{F})}(X)\big|, \tag{4}$$

where $\det J_{(\mathrm{id}-\mathbf{D}\mathrm{F})}(X)$ denotes the determinant of the vector-valued Jacobian matrix of the function $(\mathrm{id}-\mathbf{D}\mathrm{F})$ at X. See a proof in Appendix B.1.

Missing Data Model. Given sampled data on X, let $R = (R_1, \ldots, R_K)$ be the vector of binary missingness indicators with $R_k = 1$ if X_k is observed and $R_k = 0$ if X_k is missing. We only observe a coarsened version of X_k, denoted by Y_k, which is deterministically defined as $Y_k = X_k$ when $R_k = 1$, and $Y_k = ?$ if $R_k = 0$. Let $Y = (Y_1, \ldots, Y_K)$ denote the coarsened variables. Additionally, we have access to $S = (S_1, \ldots, S_K)$ where S_k is a binary indicator of intervention, such that $S_k = 0$ if X_k is intervened on (i.e., $X_k \in X_{\mathcal{I}}$), and $S_k = 1$ otherwise. We assume we have n i.i.d. copies of (Y, R, S), and the dataset is denoted by $\mathcal{D} = \{y^{(i)}, r^{(i)}, s^{(i)}\}_{i=1}^n$, where $y^{(i)}, r^{(i)}, s^{(i)}$ represent the i-th observed values of Y, R, S.

We define a missing data model as the collection of distributions over the variables X, R, Y. By chain rule of probabilities, we can express $p(X, R, Y)$ as $p(X)\, p(R|X)\, p(Y|X, R)$. We refer to $p(X)$ as the *target law*, $p(R|X)$ as the *missingness mechanism*, $p(X, R)$ as the *full law*, while $p(Y|X, R)$ is the *coarsening mechanism*, which is deterministically defined. Borrowing ideas from the graphical models of missing data (Mohan et al., 2013; Nabi et al., 2025), we use graphs to encode assumptions about $p(X, R, Y)$. Specifically, we assume that the relations between variables in the target law $p(X)$ are directed and can include cycles, and the missingness mechanism $p(R|X)$ factorizes according to a DAG, where $\text{pa}_{\mathcal{G}}(R_k)$ can only be a subset of X and $R \setminus R_k$. Finally, due to deterministic relations, Y_k has only two parents R_k and X_k. We denote these graphs by $\mathcal{G}_m = (V, \mathcal{E}_m)$, where $V = (X, R, Y)$, and $\mathcal{E}_m$ denotes the set of directed edges in the missing data graph. Two examples of missing data graphs (or m-graphs), with $K = 3$ substantive variables, are provided in Figure 1; deterministic relations are drawn in gray.

Graphically, an MCAR mechanism has no incoming edges into any missingness indicator in R, a MAR mechanism has parents of missingness indicators that are fully observed, and an MNAR mechanism involves missingness indicators with parents in X. Identifying the full or target law in an m-graph with MNAR mechanisms from observational data is not always possible. Previous work has extensively studied identification in graphical models of missing data (Bhattacharya et al., 2020; Nabi et al., 2020; Mohan & Pearl, 2021; Guo et al., 2023; Nabi et al., 2025). Nabi et al. (2020) have shown that the full law in an m-graph is identified *if and only if* there are no edges of the form $X_k \to R_k$ (no *self-censoring*) and $X_j \to R_k \leftarrow R_j$ (no *colluders*). Therefore, we restrict the m-graphs considered in this work to be identifiable (formalized in Assumption 1).

Assumption 1. *The missing data graphs under consideration have no edges of the form $X_k \to R_k$ (no* self-censoring*) and $X_j \to R_k \leftarrow R_j$ (no* colluders*).*

Given partially observed data from a set of interventional experiments, our objective is to learn the underlying full law that generated the sample. Specifically, this involves learning both the underlying target law and the missingness mechanism.

3 The MissNODAG Framework

We assume the target law $p(X)$ and the missingness mechanism $p(R|X)$ are parameterized by finite vectors θ and ϕ, respectively. Thus, we write the full law $p(X, R)$ as $p(X, R|\theta, \phi) = p(X|\theta)\ p(R|X, \phi)$. In order to learn the full law, we proceed by maximizing the log-likelihood of the observed data law.

Let $\Gamma_i = \{k : r_k^{(i)} = 1\}$ and $\Omega_i = \{k : r_k^{(i)} = 0\}$ represent the sets of indices for the variables that are observed and missing, respectively, in the i-th sample; thus $y^{(i)} = x_{\Gamma_i}^{(i)}$. Consequently, the observed data law $p\big(x_{\Gamma_i}^{(i)}, r^{(i)}\big)$ can be written down as

$$p\big(x_{\Gamma_i}^{(i)}, r^{(i)} \mid \theta, \phi\big) = \int p\big(x_{\Gamma_i}^{(i)}, x_{\Omega_i}^{(i)}, r^{(i)} \mid \theta, \phi\big)\ dx_{\Omega_i}^{(i)}. \tag{5}$$

This integration is generally intractable due to marginalization over missing variables and the lack of a closed-form solution. We address this intractability in maximizing the observed data likelihood when data is generated from an m-graph, as described in Section 2. First, we provide an overview of the MissNODAG framework, followed by details on computing the log-likelihood for missing and observed variables, and discuss imputing the missing variables under linear and nonlinear SEMs.

3.1 Score Function

Assuming the data $\mathcal{D} = \{y^{(i)}, r^{(i)}, s^{(i)}\}_{i=1}^n$ is generated from an experiment where the full law $p(X, R)$ is represented via m-graphs, our goal is to learn the entire m-graph structure by maximizing, $\tilde{\mathcal{L}}(\mathcal{D}, \theta, \phi)$, a regularized log-likelihood of the observed data law:

$$\max_{\theta,\phi} \sum_{i=1}^{n} \log p\big(x_{\Gamma_i}^{(i)}, r^{(i)} | \theta, \phi\big) - \lambda_1 \mathcal{R}(\theta) - \lambda_2 \mathcal{R}(\phi) \quad \text{s.t.} \quad h_1(\phi) = 0 \quad \text{and} \quad h_2(\phi) = 0, \tag{6}$$

where $\mathcal{R}(\cdot)$ is a regularization function that promotes sparsity, λ_1, λ_2 are regularization parameters, and the functions $h_1(\phi)$ and $h_2(\phi)$ are functions that restrict the missingness mechanism to the class of identifiable MNAR mechanisms, see Section 3.3.3 for more details.

Given a family of M interventional experiments with targets $\{X_{\mathcal{I}_m}\}_{m=1}^M$, under the population (infinite data) setting, the regularized observed data likelihood score for an m-graph $\mathcal{G}_m$, denoted as $\mathcal{S}(\mathcal{G}_m)$ is given by

$$\mathcal{S}(\mathcal{G}_m) := \sup_{\theta_{\mathcal{G}_m}, \phi_{\mathcal{G}_m}} \sum_{m=1}^{M} \mathbb{E}_{(X_\Gamma, R)\sim p_{\text{obs}}^{(m)}} \log p(X_\Gamma, R) - \lambda |\mathcal{G}_m|, \tag{7}$$

where $p_{\text{obs}}^{(m)}$ is the true data generating distribution for the m-th interventional setting, $|\mathcal{G}_m|$ denotes sparsity regularization on the m-graph, and λ denotes the combined sparsity regularization parameter. The following theorem establishes that, under appropriate assumptions, the exact maximization of $\mathcal{S}(\mathcal{G})$ results in a graph $\hat{\mathcal{G}}_m$ that is in the same Markov equivalence class as the ground truth graph $\mathcal{G}_m^*$. Formally,

Theorem 2. *Let $\{X_{\mathcal{I}_m}\}_{m=0}^M$ be a family of interventional targets, let $\mathcal{G}_m^*$ denote the ground truth directed mixed graph, $p^{(m)}$ denote the data generating distribution for $X_{\mathcal{I}_m}$, and $\hat{\mathcal{G}}_m := \arg\max_{\mathcal{G}_m \in \mathcal{G}_{id}} \mathcal{S}(\mathcal{G}_m)$, where $\mathcal{G}_{id}$ denotes the set of all m-graph that obey Assumption 1. Then, under the Assumptions 1, B.6, B.7, B.8, and B.10, and for a suitably chosen $\lambda > 0$, we have that $\hat{\mathcal{G}}_m \equiv_{\mathcal{I}} \mathcal{G}_m^*$. That is, $\hat{\mathcal{G}}_m$ is $\mathcal{I}$-Markov equivalent to $\mathcal{G}_m^*$.*

The proof for Theorem 2 is provided in Appendix B.3. This result extends the consistency guarantee established by Sethuraman & Fekri (2025) for complete data to the missing data setting. While exact maximization of the score function theoretically guarantees recovery of the ground truth Markov equivalence class, it is computationally infeasible in practice. Consequently, we resort to an Expectation-Maximization (EM) algorithm to optimize the score function (detailed in Subsection 3.2). Although EM does not strictly maximize the observed data likelihood—limiting convergence to a stationary point—our experiments indicate that MissNODAG is capable of recovering the true target law graph when provided with all single-node interventions (see Section 4).

3.2 The Overall Procedure

As discussed, computing $p(x_{\Gamma_i}^{(i)}, r^{(i)} | \theta, \phi)$ is generally intractable, with no closed-form solution. However, equation 6 can be solved using the iterative penalized expectation-maximization (EM) method (Chen et al., 2014). Unlike imputation methods that directly sample missing values, the EM algorithm starts with an initial parameter $\Theta^0 = (\theta^0, \phi^0)$ and alternates between the following two steps at iteration t until convergence:

E-step: Use the current estimates of the model parameters, $\Theta^t = (\theta^t, \phi^t)$, and the non-missing data to compute the expected log-likelihood of the full data, denoted by $\mathcal{Q}(\Theta|\Theta^t)$, and given by:

$$\mathcal{Q}(\Theta \mid \Theta^t) = \sum_{i=1}^{n} \mathbb{E}_{x_{\Omega_i}^{(i)} \sim p(\cdot | x_{\Gamma_i}^{(i)}, r^{(i)}, \Theta^t)} \Big[\log p\big(x_{\Gamma_i}^{(i)}, x_{\Omega_i}^{(i)}, r^{(i)} \mid \Theta\big) \Big]. \tag{8}$$

M-step: Maximize $\mathcal{Q}(\Theta|\Theta^t)$, computed in the E-step, with respect to Θ:

$$\Theta^{t+1} = \arg\max_{\Theta} \ \mathcal{Q}(\Theta \mid \Theta^t) - \lambda_1 \mathcal{R}(\theta) - \lambda_2 \mathcal{R}(\phi) \quad \text{s.t.} \quad h_1(\phi) = 0 \quad \text{and} \quad h_2(\phi) = 0. \tag{9}$$

We use stochastic gradient-based solvers to solve the maximization problem, alternating between updating the parameters of the target law, θ, and the parameters of the missingness mechanism, ϕ. Note that,

$$\sum_{i=1}^{n} \log p(x_{\Gamma_i}^{(i)}, r^{(i)} \mid \Theta) \geq \mathcal{Q}(\Theta \mid \Theta^t) - \text{const}. \tag{10}$$

This inequality indicates that we maximize a lower bound of the log-likelihood as we update the parameters during the M-step. More details on the derivation of equation 10 and on the convergence analysis of MissNODAG are provided in Appendix B.2.

3.3 Computational Details of the E-step

Computing the expected log-likelihood in the E-step can be challenging for a directed (cyclic) graph. First, let's look at $\log p\big(x^{(i)}_{\Gamma_i}, x^{(i)}_{\Omega_i}, r^{(i)}|\Theta\big)$ in equation 8, which equals:

$$\log p_X\left(x^{(i)}_{\Gamma_i}, x^{(i)}_{\Omega_i}|\theta\right) + \log p\big(r^{(i)}|x^{(i)}_{\Omega_i}, x^{(i)}_{\Gamma_i}, \phi\big). \tag{11}$$

3.3.1 Target Law

As per equation 4, computing $\log p_X(X|\theta)$ in equation 11 requires:

$$\log\big|\det J_{(\mathrm{id}-\mathbf{D}\mathrm{F})}(X)\big|. \tag{12}$$

In the worst case, the Jacobian matrix may require gradient calls in the order of K^2. To that end, following Sethuraman et al. (2023), we employ *contractive residual flows* (Behrmann et al., 2019; Chen et al., 2019) to compute the log-determinant of the Jacobian in a tractable manner.

Modeling the SEM in equation 2. We assume the SEM functions in $\mathrm{F}(X)$ in equation 2 are Lipschitz with Lipschitz constant less than one. Such functions are called *contractive functions*. It then follows from *Banach fixed point* theorem (Rudin, 1953) that the mapping function $(\mathrm{id}-\mathbf{D}\mathrm{F})$ is contractive and invertible.

We use neural networks to model the contractive functions in $\mathrm{F}(X)$. As shown by Behrmann et al. (2019), neural networks can be constrained to be contractive during the training phase by rescaling the layer weights by their corresponding spectral norm. While contractivity is a sufficient condition for the existence of $(\mathrm{id}-\mathrm{F})^{-1}$, it is not necessary. When the underlying graph governing the target law $p(X)$ is a DAG, it is possible to have non-contractive functions in $\mathrm{F}(X)$ for which $(\mathrm{id}-\mathrm{F})^{-1}$ exists; see (Sethuraman et al., 2023) for more details.

Naive implementation of a neural network may not produce promising results as it may introduce self-cycles. To circumvent this issue and simultaneously add sparsity penalization, we introduce a *dependency mask* matrix $\boldsymbol{M} \sim \{0,1\}^{K\times K}$ to explicitly encode the dependencies between the nodes in the graph, with zero diagonal entries to mask out the self-loops. Thus the SEM model $F(X)$ takes the following form

$$[\mathrm{F}_\theta(X)]_k = [\mathrm{NN}_\theta(M_{*,k} \odot X)]_k, \tag{13}$$

where NN_θ denotes a fully connected neural network function with parameters θ, $M_{*,k}$ denotes the k-th column of $\boldsymbol{M}$, and $\odot$ denotes the Hadamard product. The dependency mask is sampled from Gumbel-softmax distribution (Jang et al., 2016), $\boldsymbol{M} \sim p(\boldsymbol{M}|\theta)$ and the parameters θ are updated during the training (M-step). In this case, the sparsity penalty $\mathcal{R}(\theta)$ in equation 6 is set as an L1 norm, i.e., $\mathcal{R}(\theta) = \mathbb{E}_{\boldsymbol{M}\sim p(\cdot|\theta)}\|\boldsymbol{M}\|_1$.

Computing the log-determinant in equation 12. We note that $\log\big|\det J_{(\mathrm{id}-\mathbf{D}\mathrm{F})}(X)\big| = \log\big|\det(\mathbf{I} - \mathbf{D}J_{\mathrm{F}})(X)\big|$, where $\mathbf{I}$ is the $K\times K$ identity matrix. Thus, the log-determinant of the Jacobian matrix can be computed using an unbiased estimator based on the power series expansion introduced by Behrmann et al. (2019),

$$\log\Big|\det J_{(\mathrm{id}-\mathbf{D}\mathrm{F})}(X)\Big| = \log\big|\mathbf{I} - J_{\mathbf{D}\mathrm{F}}\big| = -\sum_{m=1}^{\infty}\frac{1}{m}\mathrm{Tr}\Big\{J^m_{\mathbf{D}\mathrm{F}}(X)\Big\}, \tag{14}$$

where $J^m_{\mathbf{D}\mathrm{F}}(X)$ denotes the Jacobian matrix to the m-th power. equation 14 is guaranteed to converge when $\mathrm{F}(X)$ is contractive (Hall, 2013). In practice, equation 14 is computed by truncating the number of terms in the summation to a finite number. This, however, introduces bias in estimating the log-determinant of the Jacobian. In order to circumvent this issue we follow the steps taken by Chen et al. (2019). The power series expansion is truncated at a random cut-off $N \sim p_{\mathbb{N}}(N)$, where $p_{\mathbb{N}}$ is a probability distribution over the set of natural numbers $\mathbb{N}$. Each term in the finite power series is then re-weighted to obtain the following estimator:

$$\log\big|\det J_{(\mathrm{id}-\mathbf{D}\mathrm{F})}(X)\big| = -\mathbb{E}_N\left[\sum_{m=1}^{N}\frac{\mathrm{Tr}\big\{J^m_{\mathbf{D}\mathrm{F}}(X)\big\}}{m\cdot P_{\mathbb{N}}(\ell\geq m)}\right] \tag{15}$$

Algorithm 1 IMPUTE-REJECTION

Require: Minibatch data $\mathcal{B} = \{y^{(i)}, r^{(i)}, s^{(i)}\}_{i=1}^{n_B}$, with sampling distribution $q(x)$.
Ensure: Imputed data $\tilde{\mathcal{B}} = \{\widehat{x}^{(i)}, r^{(i)}, s^{(i)}\}_{i=1}^{n_B}$.
1: **for** $i = 1$ to n_B **do**
2: Sample $\tilde{x}_{\Omega_i}^{(i)} \sim q(x_{\Omega_i})$.
3: Pick $u \sim U[0, 1]$.
4: **if** $u \leq \frac{p(\tilde{x}_{\Omega_i}^{(i)}, y_{\Gamma_i}^{(i)}|\theta^t)p(r^{(i)}|\tilde{x}_{\Omega_i}^{(i)}, y_{\Gamma_i}^{(i)}, \phi^t)}{c_0 q(\tilde{x}_{\Omega_i}^{(i)})}$ **then**
5: Accept sample: $\widehat{x}_{\Omega_i}^{(i)} = \tilde{x}_{\Omega_i}^{(i)}$; $\widehat{x}_{\Gamma_i}^{(i)} = y_{\Gamma_i}^{(i)}$.
6: **end if**
7: **end for**
return $\tilde{\mathcal{B}} = \{\widehat{x}^{(i)}, r^{(i)}, s^{(i)}\}_{i=1}^{n_B}$

where $P_{\mathbb{N}}$ is the cumulative density function of $p_{\mathbb{N}}$. Gradient calls are still required in the order of K. We can reduce this further by using the Hutchinson trace estimator (Hutchinson, 1989), where $W \sim \mathcal{N}(0, \mathbf{I})$:

$$\mathrm{Tr}\Big\{J^m_{\mathbf{D}\mathrm{F}}(X)\Big\} = \mathbb{E}_W\Big[W^\top J^m_{\mathbf{D}\mathrm{F}}(X)W\Big], \tag{16}$$

We note that the remainder of equation 4 can be efficiently computed with a forward pass of the neural network.

3.3.2 Calculating Expectation via Imputation

Combining equations 4, 8, 15, and 16, we arrive at

$$\mathcal{Q}(\Theta|\Theta^t) \propto \sum_{i=1}^{n} \mathbb{E}_{x_{\Omega_i}^{(i)}|x_{\Gamma_i}^{(i)}, r^{(i)}; \Theta^t} \left\{ \log p\Big(r^{(i)}|x_{\Omega_i}^{(i)}, x_{\Gamma_i}^{(i)}, \phi\Big) + \log p_{\epsilon_{\mathcal{O}}}\Big(\epsilon_{\mathcal{O}_i}^{(i)}\Big) - \mathbb{E}_{N,W}\left[\sum_{m=1}^{N} \frac{W^\top J^m_{\mathbf{D}\mathrm{F}}(x^{(i)})W}{m \cdot P_{\mathbb{N}}(\ell \geq m)}\right]\right\},$$

where $\epsilon^{(i)} = (\mathrm{id} - \mathbf{D}_i \mathrm{F})(x^{(i)})$, $\mathbf{D}_i$ is the diagonal matrix corresponding to the interventional mask for the i-th sample, i.e., $\mathbf{D}_i = \mathrm{diag}(s_1^{(i)}, \ldots, s_K^{(i)})$.

The expectation in the approximation for $\mathcal{Q}(\Theta|\Theta^t)$ generally lacks a closed-form solution. Therefore, it must be approximated by the sample mean, using samples drawn from the posterior distribution $p(x_{\Omega_i}^{(i)}|x_{\Gamma_i}^{(i)}, r^{(i)}, \Theta^t)$. This presents two main challenges: (i) the posterior distribution may not have a closed form, and (ii) direct sampling may be infeasible even when the posterior distribution can be evaluated. The difficulty arises due to the presence of nonlinear relations in $\mathrm{F}(X)$ and the missingness mechanism $p(r^{(i)}|x_{\Omega_i}^{(i)}, x_{\Gamma_i}^{(i)}, \phi^t)$, which may preclude straightforward sampling. Therefore, we employ *rejection sampling* (Koller & Friedman, 2009) to draw samples from a proposal distribution $q(x_{\Omega_i}^{(i)})$, from which samples can be readily generated.

To that end, a constant $c_0 > 0$ is chosen such that $c_0 q(x_{\Omega_i}^{(i)}) \geq p(x_{\Omega_i}^{(i)}|x_{\Gamma_i}^{(i)}, r^{(i)}, \Theta^t)$ for all $i = 1, \ldots, n$. However, as stated earlier the posterior distribution is not readily available. Thus, from Bayes rule, we have

$$p(x_{\Omega_i}^{(i)}|x_{\Gamma_i}^{(i)}, r^{(i)}, \Theta^t) = \frac{p(x_{\Omega_i}^{(i)}, x_{\Gamma_i}^{(i)}|\theta^t)p(r^{(i)}|x_{\Omega_i}^{(i)}, x_{\Gamma_i}^{(i)}, \phi^t)}{p(x_{\Gamma_i}^{(i)}, r^{(i)}|\Theta^t)},$$

where the denominator $p(x_{\Gamma_i}^{(i)}, r^{(i)}|\Theta^t)$ can be evaluated using fully observed data. The first term in the numerator can be computed efficiently, as discussed in Section 3.3.1. The second term is addressed in Section 3.3.3. Before that, we explain how these calculations simplify under more restrictive models. The imputation procedure is summarized in Algorithm 1. In our implementation, it is possible that one pass of rejection sampling may not yield enough samples. Thus, we repeat the rejection sampling procedure until we recover at least half of the batch.

3.3.3 Missingness Mechanism

In order to compute the log-likelihood in the E-step, we also need to compute $\log p\big(r^{(i)}|x_{\Omega_i}^{(i)}, x_{\Gamma_i}^{(i)}, \phi\big)$, which according to m-graphs can be factorized as

$$p(R \mid X, \phi) = \prod_{k=1}^{K} p\big(R_k \mid \mathrm{pa}_{\mathcal{G}_m}(R_k), \phi_k\big). \tag{17}$$

In developing MissNODAG, we focus on a class of MNAR models, where for any $R_k \in R$, $\mathrm{pa}_{\mathcal{G}_m}(R_k) \subseteq X \cup R \setminus X_k, R_k$. According to the results in Nabi et al. (2020), the full law under any MNAR mechanism that follows Assumption 1 (i.e, no self-censoring edges and no colluder structures) is identified as a function of the observed data distribution. Figure 1 provides two examples of identifiable MNAR mechanisms with $K = 3$ variables.

Under this MNAR class, each conditional factor in the missingness selection mechanism $p(R|X, \phi)$ is modeled using the expit function, with $\phi_k = \{w_k, z_k\}$:

$$p\big(R_k = 0 \mid \mathrm{pa}_{\mathcal{G}_m}(R_k), \phi_k\big) = \mathrm{expit}\big((W_{XR})^{\top}_{*,k} X + (W_{RR})^{\top}_{*,k} R + z_k\big), \tag{18}$$

where $\mathrm{expit}(x) = 1/(1 + e^{-x})$, $\mathbf{W}_{XR}$ and $\mathbf{W}_{RR}$ denote the adjacency matrix corresponding to the edges between X to R and R to R respectively. Maximization during the M-step with respect to ϕ reduces to solving a constrained sparsity-regularized logistic regression, with our choice of $\mathcal{R}(\phi) = \sum_{k=1}^{K} \|w_k\|_1$.

Identifiable MNAR mechanisms are particularly well-suited for modeling missingness in cross-sectional studies, surveys, and retrospective analyses. Consider, for instance, a study examining the relationship between smoking (X_1), tar accumulation in the lungs (X_2), and a bronchitis diagnosis (X_3), where missing entries are indicated by R_1, R_2, and R_3, respectively (see Figure 1). The edge $X_3 \to R_1$ reflects that a suspected diagnosis of bronchitis increases the likelihood of inquiring about smoking history. Smokers are more likely to undergo tests for both tar accumulation and bronchitis, represented by $R_2 \leftarrow X_1 \to R_3$. Moreover, requesting a diagnostic test for bronchitis increases the likelihood of testing for tar, which in turn makes it more likely that smoking status will be queried—captured by $R_1 \leftarrow R_2 \leftarrow R_3$ in Figure 1(b); while in the absence of such a dependency, Figure 1(a) is most suitable to illustrate the missingness mechanism.

To ensure that the model class adheres to identifiable MNAR missingness mechanisms, we explicitly incorporate the identifiability conditions (Assumption 1) into the optimization objective. The first condition, no self-censoring, can be enforced by masking the diagonal entries of $\mathbf{W}_{XR}$. The second condition, no colluders, requires more care: we must avoid structures of the form $X_k \to R_j \leftarrow R_k$. Here, the edge $X_k \to R_j$ corresponds to $(W_{XR})_{k,j}$, and $R_j \leftarrow R_k$ to $(W_{RR})_{k,j}$. To preclude both edges from co-occurring, we require $(W_{XR})_{k,j} \cdot (W_{RR})_{k,j} = 0$ for all $k, j \in [K]$. Define $h_1(\phi) = \|\mathbf{W}_{XR} \odot \mathbf{W}_{RR}\|_1$, where $\odot$ denotes the Hadamard product. Then enforcing $h_1(\phi) = 0$ guarantees the no-colluder condition, as formalized below:

Proposition 3. *Setting $h_1(\phi) = 0$ is equivalent to requiring $(W_{XR})_{k,j} \cdot (W_{RR})_{k,j} = 0$ for all $k, j \in [K]$.*

Proof. This equivalence follows directly by expanding the ℓ_1-norm in h_1; Note that,

$$h_1(\phi) = \|\mathbf{W}_{XR} \odot \mathbf{W}_{RR}\|_1 = \sum_{k,j=1}^{K} |(W_{XR})_{k,j} \cdot (W_{RR})_{k,j}|. \tag{19}$$

Setting h_1 to zero in equation 19 implies that for each $k, j \in [K]$, $(W_{XR})_{k,j} \cdot (W_{RR})_{k,j} = 0$. □

Beyond the identifiability conditions, we require the missingness indicators to lie outside any cycles—that is, the graph encoding $p(R \mid X)$ must form a directed acyclic graph (DAG). Our parameterization of the missingness mechanism precludes edges of the form $R_j \to X_i$, so it suffices to constrain $\mathbf{W}_{RR}$ to the space of DAGs. This can be achieved using the trace-exponential acyclicity constraint proposed in Zheng et al. (2018), namely, $h_2(\phi) = \mathrm{Tr}(e^{\mathbf{W}_{RR} \odot \mathbf{W}_{RR}}) - K = 0$. In summary, during the M-step, the missingness mechanism parameters are updated by solving the following constrained optimization problem:

$$\begin{aligned} \min_{\phi} \quad & -\sum_{i=1}^{n} \mathbb{E}_{x^{(i)}_{\Omega_i} \sim p(\cdot \mid x^{(i)}_{\Gamma_i}, r^{(i)}, \Theta^t)} \left[\log p\left(r^{(i)} \mid x^{(i)}_{\Gamma_i}, x^{(i)}_{\Omega_i}, \phi\right)\right] \\ \text{subject to} \quad & \underbrace{\|\mathbf{W}_{XR} \odot \mathbf{W}_{RR}\|_1 = 0}_{h_1(\phi)\text{: no colluders constraint}}, \quad \text{and} \quad \underbrace{\mathrm{Tr}(e^{\mathbf{W}_{RR} \odot \mathbf{W}_{RR}}) - K = 0}_{h_2(\phi)\text{: DAG constraint}}. \end{aligned}$$

Parameter update via Augmented Lagrangian. Following Zheng et al. (2018), we use the augmented Lagrangian method to solve the constrained optimization problem above. This approach augments the original objective with a quadratic penalty, yielding:

$$\begin{aligned} \min_{\phi} \quad & -\sum_{i=1}^{n} \mathbb{E}_{x_{\Omega_i}^{(i)} \sim p(\cdot \mid x_{\Gamma_i}^{(i)}, r^{(i)}, \Theta^t)} \left[\log p \left(r^{(i)} \mid x_{\Gamma_i}^{(i)}, x_{\Omega_i}^{(i)}, \phi \right) \right] + \frac{\rho}{2} \sum_{i=1}^{2} h_i(\phi) \\ \text{subject to} \quad & h_1(\phi) = 0, \quad \text{and} \quad h_2(\phi) = 0, \end{aligned}$$

where $\rho > 0$ is the penalty coefficient. A key advantage of the augmented Lagrangian approach is that it approximates the solution to the constrained problem without requiring ρ to tend to infinity. This allows us to reformulate the objective as an unconstrained problem:

$$\min_{\phi} -\sum_{i=1}^{n} \mathbb{E}_{x_{\Omega_i}^{(i)} \sim p(\cdot \mid x_{\Gamma_i}^{(i)}, r^{(i)}, \Theta^t)} \left[\log p \left(r^{(i)} \mid x_{\Gamma_i}^{(i)}, x_{\Omega_i}^{(i)}, \phi \right) \right] + \frac{\rho}{2} \sum_{i=1}^{2} h_i(\phi) + \sum_{i=1}^{2} \lambda_i h_i(\phi) \tag{20}$$

where λ_1 and λ_2 are the dual variables associated with the constraints. These are updated at each iteration via:

$$\lambda_i \leftarrow \lambda_i + \rho h_i(\phi), \quad i = 1, 2. \tag{21}$$

4 Experiments

4.1 Synthetic Experiments

Using synthetic data, we compared MissNODAG to MissDAG (`missdag`) (Gao et al., 2022), an EM-based causal discovery method limited to DAGs and MAR missingness, MVPC (Tu et al., 2019) a constraint-based method capable of handling MNAR missing data. Since MVPC does not handle interventions out-of-the-box, we apply the joint causal inference (JCI) (Mooij et al., 2020) framework along with MVPC to learn from interventional partially observed data. We also tested state-of-the-art imputation methods, including optimal transport (`optransport`) (Muzellec et al., 2020), MissForest (`missforest`) (Stekhoven & Bühlmann, 2012), and mean imputation, followed by causal graph learning from the imputed data using NODAGS-Flow (Sethuraman et al., 2023). Additionally, we also compare MissNODAG with ENCO Lippe et al. (2022) after imputing the missing data with `optransport` imputation method, see Appendix D for details on the implementation of MissNODAG and the baselines. Note that, ENCO, MissDAG, and MVPC are only capable of learning DAGs, putting these methods at a disadvantage compared to the other baselines. Moreover, MissDAG doesn't handle MNAR missingness.

In all experiments, we generated cyclic directed graphs with K=10 nodes using the Erdős-Rényi (ER) random graph model. For linear SEMs, edge weights were uniformly sampled from $(-0.6, -0.25) \cup (0.25, 0.6)$ and rescaled to ensure contractivity. For nonlinear SEMs, the causal mechanism was defined as $F(X) = \tanh(\mathbf{W}^\top X)$, where the nonzero entries of $\mathbf{W}$ were drawn from the same distribution and similarly rescaled for contractivity. Exogenous noise variables were sampled from a Gaussian distribution with standard deviations randomly chosen between 0.1 and 0.3. The m-graph was generated using the ER model, followed by postprocessing to enforce acyclicity in $\mathbf{W}_{RR}$. Missingness mechanism edge weights were sampled from a standard normal distribution. The training data comprised single-node interventional experiments for all nodes in the target graph (unless specified otherwise). Upon creation of the clean data, some of the observations are replaced with "?" (indicating missing value) based on the missingness mechanism modeled by the m-graph. We evaluated MissNODAG and baseline methods across the following five settings.

Sensitivity missing probability. The average probability of a node being missing ($\mathbb{E}[R_i]$) is varied between 0.1 and 0.5. Each interventional setting consists of 1000 samples. Additionally, the outgoing edge densities of the target law and the missingness mechanism are set to 2 and 3 respectively.

Sensitivity to nonlinearity. We varied the degree of nonlinearity by adjusting $\beta \in [0, 1]$ in:

$$X = (1 - \beta)\mathbf{W}^\top X + \beta \tanh(\mathbf{W}^\top X) + \epsilon. \tag{22}$$

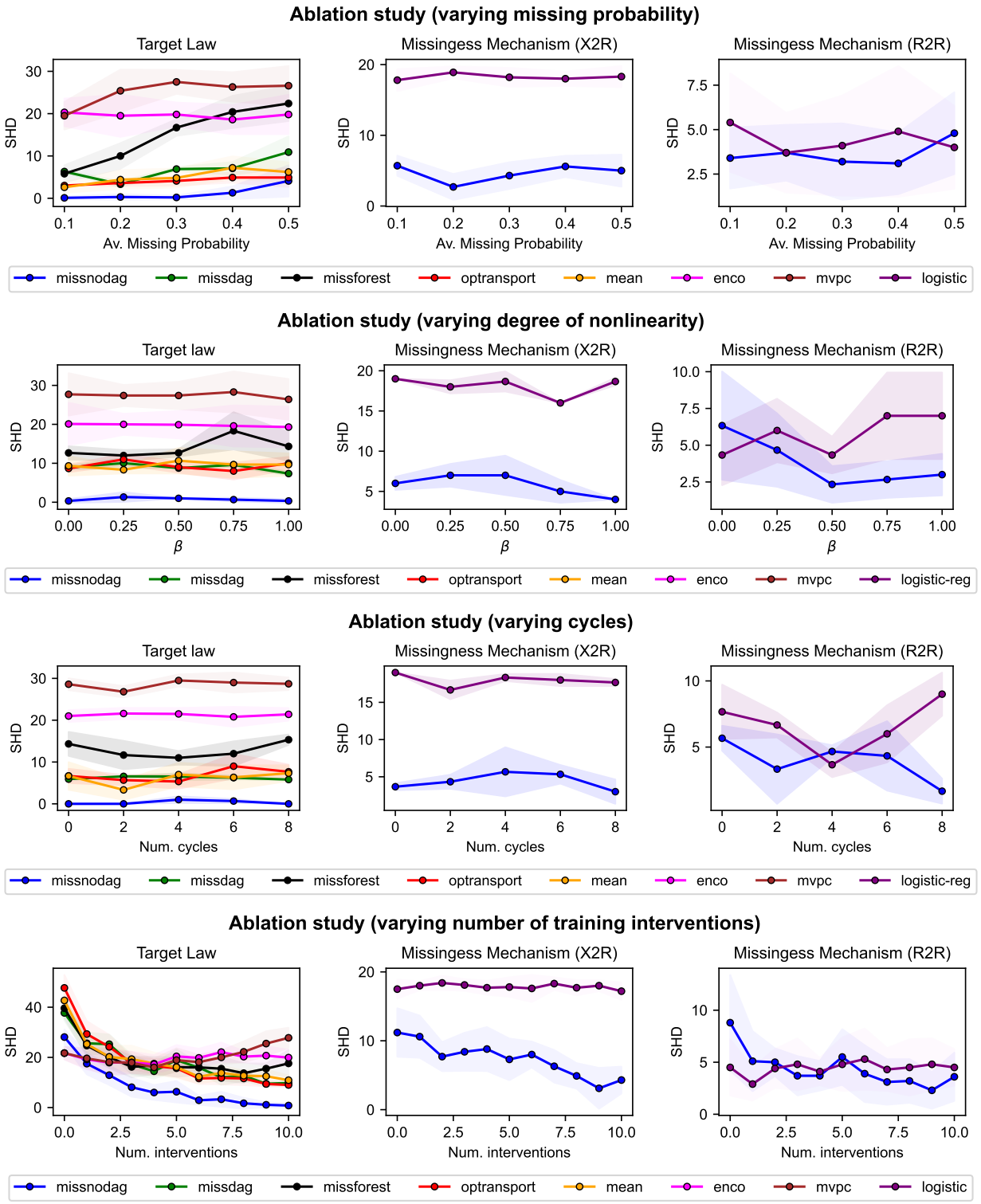

Figure 2: Performance comparison on synthetic data

Here, $\beta = 0$ corresponds to a fully linear SEM, and $\beta = 1$ to a fully nonlinear SEM. The number of nodes in the target law graph K was set to 10, missing probability set to 0.3, and the number of cycles were randomly chosen.

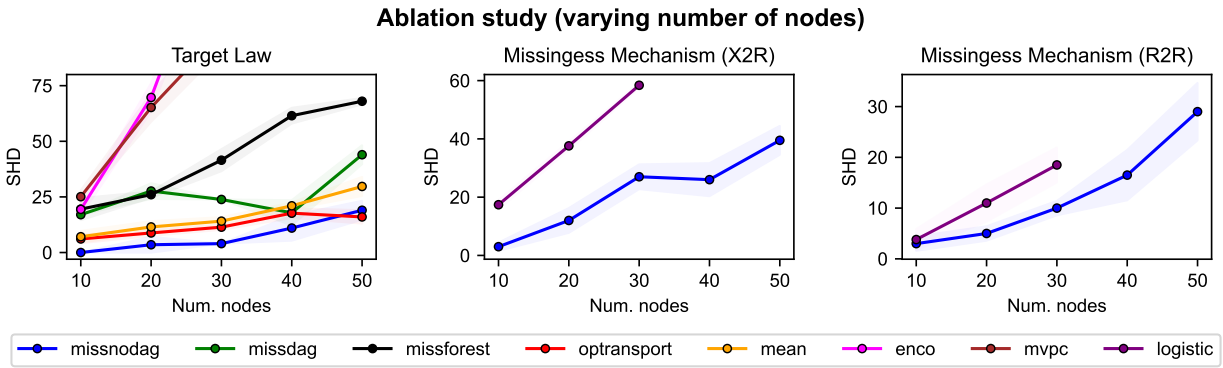

Figure 3: Performance comparison between MissNODAG and the baselines as a function of the number of nodes in the target law graph.

Sensitivity to cycles. We varied the number of cycles in the target-law graph from 0 to 8, fixing the number of nodes at $K = 10$ and setting $\beta = 1$ in equation 22. The missing probability was set to 0.3.

Sensitivity to training interventions. We varied the number of interventions provided during the training phase. Starting from 0 interventional experiments in the training set (corresponding to observational setting) to all single-node interventional experiments (10 interventions). Here K was set to 10, missing probability to 0.3, $\beta = 1.0$ in equation 22.

Sensitivity to number of nodes. In this case, the number of nodes in the target law graph was varied between 10 and 30, with the number of cycles assigned at random and $\beta = 1$ in equation 22. The missing probability was set to 0.3.

Structural Hamming distance (SHD) is used as the error metric to compare MissNODAG with the baselines. SHD counts the number of operations (addition, deletion, and reversal) needed to match the estimated graph to the ground truth.

Target law recovery. We first analyze target law recovery performance, summarized in the left columns of Figure 2 and Figure 3. Across all five settings, MissNODAG either outperforms or matches the baselines. In the experiment with varying missingness probabilities (Figure 2, top row), the performance of all methods declines slightly as the average missingness probability increases; however, MissNODAG achieves nearly perfect recovery up to a missing probability of 0.3. In the second and third settings (varying nonlinearity and cycle counts), MissNODAG remains robust, achieving SHD scores close to 0. regarding the number of training interventions, MissNODAG performs competitively; while ENCO performs better in the purely observational setting (zero interventions), MissNODAG overtakes it as the number of interventions increases, widening the performance gap. Finally, regarding scalability (Figure 3), while all methods deteriorate as the graph size grows, MissNODAG remains the top-performing model for graphs up to $K = 40$ nodes.

Missingness mechanism recovery. For analyzing the missingness mechanism recovery, the baseline model applies logistic regression, treating each missingness indicator R_i as the target and using the remaining indicators R_{-i} along with X as features. We evaluate recovery in two parts: $X \to R$ edges and $R \to R$ edges. For the latter, we convert the estimated graph into its completed partially directed acyclic graph (CPDAG) and compute SHD against the ground truth CPDAG. Results for $X \to R$ edge recovery are shown in the middle column of Figure 2 and Figure 3, and for $R \to R$ edge recovery in the right column of Figure 2 and Figure 3, with baseline models denoted as `logistic`. On $X \to R$ recovery, MissNODAG consistently outperforms the baselines across all five settings, with a more pronounced performance gap than in target law recovery. For $R \to R$ recovery, MissNODAG again matches or exceeds baseline performance in all settings, though the difference is less pronounced.

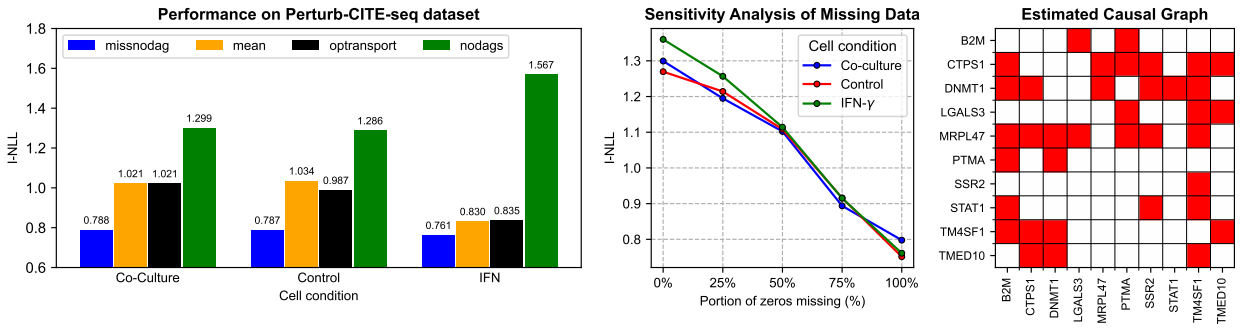

Figure 4: Evaluation on Perturb-CITE-seq gene perturbation data. (Left) Performance comparison on the Perturb-CITE-seq scRNA-seq dataset with $d = 10$ genes, measured using interventional negative log-likelihood (I-NLL). Zero gene expression values are treated as missing. (Middle) Sensitivity analysis with respect to the fraction of zero-valued gene expressions treated as missing; 0% corresponds to the fully observed setting (NODAGS-Flow). (Right) Adjacency matrix of the estimated causal graph for the co-culture cell condition, where red entries indicate the presence of a directed edge from the gene corresponding to the row to the gene corresponding to the column.

4.2 Real-World Experiment

Here we present an experiment focused on learning causal graph structure corresponding to a gene regulator network from a single-cell RNA-sequencing (*scRNA-seq*) dataset with genetic interventions. In particular, we focus on the Perturb-CITE-seq dataset (Frangieh et al., 2021), a type of data set that allows one to study causal relations in gene networks at an unprecedented scale. It contains gene expressions taken from 218,331 melanoma cells split into three cell conditions: (i) control (57,627 cells), (ii) co-culture (73,114 cells), and (iii) interferon (INF)-γ (87,590 cells).

Due to practical and computational constraints, we restrict our analysis to a subset of 10 genes (out of 20,000), following the experimental setup of Sethuraman et al. (2023), as summarized in Table 1. We include all single-gene interventions targeting this subset, treating each cell condition as an independent dataset on which models are trained separately.

Table 1: List of genes chosen from Perturb-CITE-seq dataset (Frangieh et al., 2021).

STAT1	B2M	LGALS3	PTMA
SSR2	CTPS1	TM4SF1	MRPL47
DNMT1	TMED10		

A key challenge in scRNA-seq data is the prevalence of zeros, a phenomenon known as *dropout*. While some zeros reflect true biological absence of gene expression (Zappia et al., 2017), others are technical artifacts introduced by the sequencing process (Jiang et al., 2022; Ding et al., 2020). In our work, we treat all zero expression values as missing and apply MissNODAG to impute them during training. Although this approach may misclassify genuine biological zeros as missing, we find that treating zeros as missing improves model performance compared to assuming fully observed data.

Since the data set does not provide a ground truth causal graph, it is not possible to directly compare the performance using SHD. Instead, we compare the performance of the causal discovery methods based on its predictive performance over unseen interventions. To that end, we perform a 90-10 split on the three data sets. The smaller set is treated as the test set, which is then used for performance comparison between MissNODAGS and the baselines. As a performance metric, we use the predicted negative log-likelihood (NLL) over the test set after training the models for 100 epochs. The results are summarized in Figure 4.

MissNODAG outperforms baseline methods across all three cell conditions. Furthermore, MissNODAG and other imputation-based approaches (`mean` and `optransport`) consistently surpass NODAGS-Flow trained directly on unprocessed data. The middle plot of Figure 4 presents a sensitivity analysis in which we vary the proportion of zero gene concentrations treated as missing data (dropouts) from 0% to 100%. The results indicate that predictive performance improves as a larger fraction of zero values is explicitly modeled as

dropout. These findings highlight the prevalence of dropouts in scRNA-seq datasets and underscore the critical importance of accounting for them when modeling gene expression data.

Finally, we provide the estimated gene regulatory network in Figure 4 (right). MissNODAG has successfully recovered key regulatory structures and feedback loops consistent with established T-cell biology. The directed edge STAT1 $\rightarrow$ B2M correctly identifies a primary regulatory mechanism where the transcription factor STAT1 drives the expression of antigen presentation machinery, a well-known response to immune signaling Frangieh et al. (2021). The hub of connections surrounding CTPS1 validates the model's ability to detect functional metabolic modules, as CTPS1 is the rate-limiting enzyme specifically required for T-cell proliferation and DNA synthesis Martin et al. (2014). The detected cycle between DNMT1 and STAT1 captures a sophisticated epigenetic feedback loop, where DNMT1 is required for cell division but simultaneously acts to repress STAT1 to prevent excessive inflammation, validating the method's capacity to identify cyclic causal dependencies in biological data Zhang et al. (2005).

5 DISCUSSION

In this work, we proposed MissNODAG, a novel differentiable causal discovery framework capable of learning nonlinear cyclic causal graphs along with the missingness mechanism from incomplete interventional data. The framework employs an expectation-maximization algorithm that alternates between imputing missing values and optimizing model parameters. We demonstrated how imputation can be efficiently achieved using rejection sampling, and in the case of linear SEMs with MAR missingness, by directly sampling from the posterior distribution. One of the key strengths of MissNODAG is its ability to handle cyclic directed graphs and MNAR missingness, a significant advancement over methods that typically focus on DAGs and MAR mechanisms.

MissNODAG has three primary limitations. First, our theoretical guarantees rely on strict identifiability assumptions (Assumption 1); as shown in Appendix C.2, violating these conditions degrades performance, particularly for the missingness mechanism. Second, the non-convex optimization landscape means the EM procedure guarantees convergence only to a stationary point, not a global maximum. Finally, the Jacobian log-determinant computation imposes a computational complexity of $\mathcal{O}(K^2L)$, limiting scalability to large-scale graphs.

Future research directions include: (1) incorporating realistic measurement noise models in the SEMs to enhance robustness in real-world datasets, as explored in linear DAG models by Saeed et al. (2020); (2) scaling the current framework to larger graphs using low-rank models and variational inference techniques, as explored in acyclic structures by Lopez et al. (2022); (3) allowing for unobserved confounders within the modeling assumptions, as was explored in the case of latent DAGs with complete observations by Bhattacharya et al. (2021); and (4) generalizing our framework to broader classes of identifiable MNAR models, while tackling the challenges of non-identifiability in the full or target laws, as explored in DAG models by Nabi & Bhattacharya (2023) and Guo et al. (2023).

References

Carlos Améndola, Philipp Dettling, Mathias Drton, Federica Onori, and Jun Wu. Structure learning for cyclic linear causal models. In *Conference on Uncertainty in Artificial Intelligence*, pp. 999–1008. PMLR, 2020.

Jens Behrmann, Will Grathwohl, Ricky TQ Chen, David Duvenaud, and Jörn-Henrik Jacobsen. Invertible residual networks. In *International Conference on Machine Learning*, pp. 573–582. PMLR, 2019.

Rohit Bhattacharya, Razieh Nabi, Ilya Shpitser, and James M Robins. Identification in missing data models represented by directed acyclic graphs. In *Uncertainty in artificial intelligence*, pp. 1149–1158. PMLR, 2020.

Rohit Bhattacharya, Tushar Nagarajan, Daniel Malinsky, and Ilya Shpitser. Differentiable causal discovery under unmeasured confounding. In *International Conference on Artificial Intelligence and Statistics*, pp. 2314–2322. PMLR, 2021.

Kenneth A Bollen. *Structural equations with latent variables*, volume 210. John Wiley & Sons, 1989.

Stephan Bongers, Patrick Forré, Jonas Peters, and Joris M Mooij. Foundations of structural causal models with cycles and latent variables. *The Annals of Statistics*, 49(5):2885–2915, 2021.

Philippe Brouillard, Sébastien Lachapelle, Alexandre Lacoste, Simon Lacoste-Julien, and Alexandre Drouin. Differentiable causal discovery from interventional data. *Advances in Neural Information Processing Systems*, 33:21865–21877, 2020.

Rufus Lynn Carter. Solutions for missing data in structural equation modeling. *Research & Practice in Assessment*, 1:4–7, 2006.

Lin S Chen, Ross L Prentice, and Pei Wang. A penalized em algorithm incorporating missing data mechanism for gaussian parameter estimation. *Biometrics*, 70(2):312–322, 2014.

Ricky TQ Chen, Jens Behrmann, David K Duvenaud, and Jörn-Henrik Jacobsen. Residual flows for invertible generative modeling. *Advances in Neural Information Processing Systems*, 32, 2019.

Jiarui Ding, Xian Adiconis, Sean K Simmons, Monika S Kowalczyk, Cynthia C Hession, Nemanja D Marjanovic, Travis K Hughes, Marc H Wadsworth, Tyler Burks, Lan T Nguyen, et al. Systematic comparison of single-cell and single-nucleus rna-sequencing methods. *Nature biotechnology*, 38(6):737–746, 2020.

Mathias Drton, Christopher Fox, and Y. Samuel Wang. Computation of maximum likelihood estimates in cyclic structural equation models. *The Annals of Statistics*, 47(2):663 – 690, 2019. doi: 10.1214/17-AOS1602. URL `https://doi.org/10.1214/17-AOS1602`.

Patrick Forré and Joris M Mooij. Markov properties for graphical models with cycles and latent variables. *arXiv preprint arXiv:1710.08775*, 2017.

Chris J Frangieh, Johannes C Melms, Pratiksha I Thakore, Kathryn R Geiger-Schuller, Patricia Ho, Adrienne M Luoma, Brian Cleary, Livnat Jerby-Arnon, Shruti Malu, Michael S Cuoco, et al. Multimodal pooled Perturb-CITE-seq screens in patient models define mechanisms of cancer immune evasion. *Nature genetics*, 53(3):332–341, 2021.

Jacob W. Freimer, Oren Shaked, Sahin Naqvi, Nasa Sinnott-Armstrong, Arwa Kathiria, Christian M. Garrido, Amy F. Chen, Jessica T. Cortez, William J. Greenleaf, Jonathan K. Pritchard, and Alexander Marson. Systematic discovery and perturbation of regulatory genes in human T cells reveals the architecture of immune networks. *Nature Genetics*, pp. 1–12, July 2022. ISSN 1546-1718. doi: 10.1038/s41588-022-01106-y. URL `https://www.nature.com/articles/s41588-022-01106-y`.

Nir Friedman. The bayesian structural em algorithm. In *Conference on Uncertainty in Artificial Intelligence*, 1998. URL `https://api.semanticscholar.org/CorpusID:447055`.

Alexander Gain and Ilya Shpitser. Structure learning under missing data. In *International conference on probabilistic graphical models*, pp. 121–132. PMLR, 2018.

Erdun Gao, Ignavier Ng, Mingming Gong, Li Shen, Wei Huang, Tongliang Liu, Kun Zhang, and Howard Bondell. Missdag: Causal discovery in the presence of missing data with continuous additive noise models. *Advances in Neural Information Processing Systems*, 35:5024–5038, 2022.

Emily Getzen, Lyle Ungar, Danielle Mowery, Xiaoqian Jiang, and Qi Long. Mining for equitable health: Assessing the impact of missing data in electronic health records. *Journal of biomedical informatics*, 139: 104269, 2023.

Anna Guo, Jiwei Zhao, and Razieh Nabi. Sufficient identification conditions and semiparametric estimation under missing not at random mechanisms. In *Uncertainty in Artificial Intelligence*, pp. 777–787. PMLR, 2023.

Brian C. Hall. *Lie Groups, Lie Algebras, and Representations*, pp. 333–366. Springer New York, New York, NY, 2013. ISBN 978-1-4614-7116-5. doi: 10.1007/978-1-4614-7116-5_16. URL https://doi.org/10.1007/978-1-4614-7116-5_16.

Alain Hauser and Peter Bühlmann. Characterization and greedy learning of interventional markov equivalence classes of directed acyclic graphs. *The Journal of Machine Learning Research*, 13(1):2409–2464, 2012.

Christina Heinze-Deml, Jonas Peters, and Nicolai Meinshausen. Invariant causal prediction for nonlinear models. *Journal of Causal Inference*, 6(2), 2018.

Jan-Christian Huetter and Philippe Rigollet. Estimation rates for sparse linear cyclic causal models. In Jonas Peters and David Sontag (eds.), *Proceedings of the 36th Conference on Uncertainty in Artificial Intelligence (UAI)*, volume 124 of *Proceedings of Machine Learning Research*, pp. 1169–1178. PMLR, 03–06 Aug 2020. URL https://proceedings.mlr.press/v124/huetter20a.html.

Michael F Hutchinson. A stochastic estimator of the trace of the influence matrix for Laplacian smoothing splines. *Communications in Statistics-Simulation and Computation*, 18(3):1059–1076, 1989.

Antti Hyttinen, Frederick Eberhardt, and Patrik O Hoyer. Learning linear cyclic causal models with latent variables. *The Journal of Machine Learning Research*, 13(1):3387–3439, 2012.

Guido W Imbens and Donald B Rubin. *Causal inference in statistics, social, and biomedical sciences*. Cambridge University Press, 2015.

Eric Jang, Shixiang Gu, and Ben Poole. Categorical reparameterization with Gumbel-Softmax. *arXiv preprint arXiv:1611.01144*, 2016.

Ruochen Jiang, Tianyi Sun, Dongyuan Song, and Jingyi Jessica Li. Statistics or biology: the zero-inflation controversy about scrna-seq data. *Genome biology*, 23(1):31, 2022.

Diederik P Kingma and Jimmy Ba. Adam: A method for stochastic optimization. *arXiv preprint arXiv:1412.6980*, 2014.

Daphne Koller and Nir Friedman. *Probabilistic graphical models: principles and techniques*. MIT press, 2009.

Trent Kyono, Yao Zhang, Alexis Bellot, and Mihaela van der Schaar. Miracle: Causally-aware imputation via learning missing data mechanisms. *Advances in Neural Information Processing Systems*, 34:23806–23817, 2021.

Gustavo Lacerda, Peter Spirtes, Joseph Ramsey, and Patrik O. Hoyer. Discovering cyclic causal models by independent components analysis. In *Proceedings of the Twenty-Fourth Conference on Uncertainty in Artificial Intelligence*, UAI'08, pp. 366–374, Arlington, Virginia, USA, 2008. AUAI Press. ISBN 0974903949.

Hao-Chih Lee, Matteo Danieletto, Riccardo Miotto, Sarah T Cherng, and Joel T Dudley. Scaling structural learning with NO-BEARS to infer causal transcriptome networks. In *Pacific Symposium on Biocomputing 2020*, pp. 391–402. World Scientific, 2019.

Steven Cheng-Xian Li, Bo Jiang, and Benjamin Marlin. Learning from incomplete data with generative adversarial networks. In *International Conference on Learning Representations*, 2019. URL https://openreview.net/forum?id=S1lDV3RcKm.

Phillip Lippe, Taco Cohen, and Efstratios Gavves. Efficient neural causal discovery without acyclicity constraints. In *International Conference on Learning Representations*, 2022. URL https://openreview.net/forum?id=eYciPrLuUhG.

Roderick JA Little and Donald B Rubin. *Statistical analysis with missing data*, volume 793. John Wiley & Sons, 2019.

Romain Lopez, Jan-Christian Hütter, Jonathan Pritchard, and Aviv Regev. Large-scale differentiable causal discovery of factor graphs. *Advances in Neural Information Processing Systems*, 35:19290–19303, 2022.

Yonghong Luo, Xiangrui Cai, Ying Zhang, Jun Xu, et al. Multivariate time series imputation with generative adversarial networks. *Advances in neural information processing systems*, 31, 2018.

Emmanuel Martin, Noé Palmic, Sylvia Sanquer, Christelle Lenoir, Fabian Hauck, Cédric Mongellaz, Sylvie Fabrega, Patrick Nitschké, Mauro Degli Esposti, Jeremy Schwartzentruber, et al. Ctp synthase 1 deficiency in humans reveals its central role in lymphocyte proliferation. *Nature*, 510(7504):288–292, 2014.

Christopher Meek. *Graphical Models: Selecting causal and statistical models*. PhD thesis, Carnegie Mellon University, 1997.

Karthika Mohan and Judea Pearl. Graphical models for processing missing data. *Journal of the American Statistical Association*, 116(534):1023–1037, 2021.

Karthika Mohan, Judea Pearl, and Jin Tian. Graphical models for inference with missing data. In C.J. Burges, L. Bottou, M. Welling, Z. Ghahramani, and K.Q. Weinberger (eds.), *Advances in Neural Information Processing Systems*, volume 26. Curran Associates, Inc., 2013. URL `https://proceedings.neurips.cc/paper_files/paper/2013/file/0ff8033cf9437c213ee13937b1c4c455-Paper.pdf`.

Joris M Mooij and Tom Heskes. Cyclic causal discovery from continuous equilibrium data. In *Uncertainty in Artificial Intelligence*, 2013.

Joris M Mooij, Sara Magliacane, and Tom Claassen. Joint causal inference from multiple contexts. *Journal of machine learning research*, 21(99):1–108, 2020.

Boris Muzellec, Julie Josse, Claire Boyer, and Marco Cuturi. Missing data imputation using optimal transport. In *International Conference on Machine Learning*, pp. 7130–7140. PMLR, 2020.

Razieh Nabi and Rohit Bhattacharya. On testability and goodness of fit tests in missing data models. In *Uncertainty in Artificial Intelligence*, pp. 1467–1477. PMLR, 2023.

Razieh Nabi, Rohit Bhattacharya, and Ilya Shpitser. Full law identification in graphical models of missing data: Completeness results. In *International conference on machine learning*, pp. 7153–7163. PMLR, 2020.

Razieh Nabi, Rohit Bhattacharya, Ilya Shpitser, and James M. Robins. Causal and counterfactual views of missing data models. *Statistica Sinica*, 2025. doi: 10.5705/ss.202023.0382. URL `https://www3.stat.sinica.edu.tw/preprint/SS-2023-0382_Preprint.pdf`.

Ignavier Ng, AmirEmad Ghassami, and Kun Zhang. On the role of sparsity and DAG constraints for learning linear dags. *Advances in Neural Information Processing Systems*, 33:17943–17954, 2020.

Ignavier Ng, Shengyu Zhu, Zhuangyan Fang, Haoyang Li, Zhitang Chen, and Jun Wang. Masked gradient-based causal structure learning. In *Proceedings of the 2022 SIAM International Conference on Data Mining (SDM)*, pp. 424–432. SIAM, 2022.

Judea Pearl. *Causality*. Cambridge University Press, 2 edition, 2009. doi: 10.1017/CBO9780511803161.

Thomas Richardson. A discovery algorithm for directed cyclic graphs. In *Proceedings of the Twelfth international conference on Uncertainty in artificial intelligence*, pp. 454–461, 1996.

Walter Rudin. *Principles of Mathematical Analysis*. McGraw-Hill Book Company, Inc., New York-Toronto-London, 1953.

Karen Sachs, Omar Perez, Dana Pe'er, Douglas A. Lauffenburger, and Garry P. Nolan. Causal protein-signaling networks derived from multiparameter single-cell data. *Science*, 308(5721):523–529, 2005.

Basil Saeed, Anastasiya Belyaeva, Yuhao Wang, and Caroline Uhler. Anchored causal inference in the presence of measurement error. In *Conference on uncertainty in artificial intelligence*, pp. 619–628. PMLR, 2020.

Eran Segal, Dana Pe'er, Aviv Regev, Daphne Koller, Nir Friedman, and Tommi Jaakkola. Learning module networks. *Journal of Machine Learning Research*, 6(4), 2005.

Muralikrishnna G Sethuraman, Romain Lopez, Rahul Mohan, Faramarz Fekri, Tommaso Biancalani, and Jan-Christian Huetter. Nodags-flow: Nonlinear cyclic causal structure learning. In *Proceedings of The 26th International Conference on Artificial Intelligence and Statistics*, volume 206 of *Proceedings of Machine Learning Research*, pp. 6371–6387. PMLR, 25–27 Apr 2023. URL `https://proceedings.mlr.press/v206/sethuraman23a.html`.

Muralikrishnna Guruswamy Sethuraman and Faramarz Fekri. Differentiable cyclic causal discovery under unmeasured confounders. In *The Thirty-ninth Annual Conference on Neural Information Processing Systems*, 2025. URL `https://openreview.net/forum?id=95z3psF9zJ`.

Moninder Singh. Learning bayesian networks from incomplete data. *AAAI/IAAI*, 1001:534–539, 1997.

Liam Solus, Yuhao Wang, Lenka Matejovicova, and Caroline Uhler. Consistency guarantees for permutation-based causal inference algorithms. *arXiv preprint arXiv:1702.03530*, 2017.

Peter Spirtes, Clark N Glymour, Richard Scheines, and David Heckerman. *Causation, prediction, and search*. MIT press, 2000.

Daniel J Stekhoven and Peter Bühlmann. Missforest—non-parametric missing value imputation for mixed-type data. *Bioinformatics*, 28(1):112–118, 2012.

Eric V Strobl, Shyam Visweswaran, and Peter L Spirtes. Fast causal inference with non-random missingness by test-wise deletion. *International journal of data science and analytics*, 6:47–62, 2018.

John J Sulik, Nathaniel K Newlands, and Dan S Long. Encoding dependence in bayesian causal networks. *Frontiers in Environmental Science*, 4:84, 2017.

Sofia Triantafillou and Ioannis Tsamardinos. Constraint-based causal discovery from multiple interventions over overlapping variable sets. *The Journal of Machine Learning Research*, 16(1):2147–2205, 2015.

Ioannis Tsamardinos, Laura E Brown, and Constantin F Aliferis. The max-min hill-climbing bayesian network structure learning algorithm. *Machine learning*, 65(1):31–78, 2006.

Ruibo Tu, Cheng Zhang, Paul Ackermann, Karthika Mohan, Hedvig Kjellström, and Kun Zhang. Causal discovery in the presence of missing data. In *The 22nd International Conference on Artificial Intelligence and Statistics*, pp. 1762–1770. PMLR, 2019.

Guy Van den Broeck, Karthika Mohan, Arthur Choi, Adnan Darwiche, and Judea Pearl. Efficient algorithms for bayesian network parameter learning from incomplete data. In *Proceedings of the Thirty-First Conference on Uncertainty in Artificial Intelligence*, UAI'15, pp. 161–170, Arlington, Virginia, USA, 2015. AUAI Press. ISBN 9780996643108.

Yuhao Wang, Liam Solus, Karren Yang, and Caroline Uhler. Permutation-based causal inference algorithms with interventions. *Advances in Neural Information Processing Systems*, 30, 2017.

Yuhao Wang, Vlado Menkovski, Hao Wang, Xin Du, and Mykola Pechenizkiy. Causal discovery from incomplete data: a deep learning approach. *arXiv preprint arXiv:2001.05343*, 2020.

Ian R White, Patrick Royston, and Angela M Wood. Multiple imputation using chained equations: issues and guidance for practice. *Statistics in medicine*, 30(4):377–399, 2011.

C. F. Jeff Wu. On the Convergence Properties of the EM Algorithm. *The Annals of Statistics*, 11(1):95 – 103, 1983. doi: 10.1214/aos/1176346060. URL `https://doi.org/10.1214/aos/1176346060`.

Yue Yu, Jie Chen, Tian Gao, and Mo Yu. DAG-GNN: DAG structure learning with graph neural networks. In *International Conference on Machine Learning*, pp. 7154–7163. PMLR, 2019.

Luke Zappia, Belinda Phipson, and Alicia Oshlack. Splatter: simulation of single-cell rna sequencing data. *Genome biology*, 18(1):174, 2017.

Bin Zhang, Chris Gaiteri, Liviu-Gabriel Bodea, Zhi Wang, Joshua McElwee, Alexei A. Podtelezhnikov, Chunsheng Zhang, Tao Xie, Linh Tran, and Radu Dobrin. Integrated systems approach identifies genetic nodes and networks in late-onset Alzheimer's disease. *Cell*, 153(3):707–720, 2013.

Qian Zhang, Hong Y Wang, Michal Marzec, Puthiyaveettil N Raghunath, Tomohiko Nagasawa, and Mariusz A Wasik. Stat3-and dna methyltransferase 1-mediated epigenetic silencing of shp-1 tyrosine phosphatase tumor suppressor gene in malignant t lymphocytes. *Proceedings of the National Academy of Sciences*, 102(19):6948–6953, 2005.

Xun Zheng, Bryon Aragam, Pradeep K Ravikumar, and Eric P Xing. DAGs with NO TEARS: Continuous optimization for structure learning. In S. Bengio, H. Wallach, H. Larochelle, K. Grauman, N. Cesa-Bianchi, and R. Garnett (eds.), *Advances in Neural Information Processing Systems*, volume 31, 2018. URL `https://proceedings.neurips.cc/paper/2018/file/e347c51419ffb23ca3fd5050202f9c3d-Paper.pdf`.

Xun Zheng, Chen Dan, Bryon Aragam, Pradeep Ravikumar, and Eric Xing. Learning sparse nonparametric DAGs. In Silvia Chiappa and Roberto Calandra (eds.), *Proceedings of the Twenty Third International Conference on Artificial Intelligence and Statistics*, volume 108, pp. 3414–3425, 26–28 Aug 2020.

Appendix

The appendix is structured as follows. **Appendix A** offers a summary of the notations used throughout the manuscript for ease of reference. **Appendix B** contains all the proofs. **Appendix C** provides details on three sets of additional simulations and a comparison of training times. **Appendix D** provides additional details on the implementation of the baselines and the MissNODAG framework.

A GLOSSARY

A comprehensive list of notations used in the manuscript is provided in Table 2.

Table 2: Glossary of terms and notations

Symbol	Definition	Symbol	Definition
X, x	Variables, values	$\mathcal{G}, \mathcal{G}_m$	Graph, m-graph
ϵ	Exogenous noise terms	k	Graph node index variable
R	Missingness indicators	K	Total nodes in $\mathcal{G}$
Y	Coarsened version of X	$\text{pa}_{\mathcal{G}}(X_k)$	Parent set of X_k in $\mathcal{G}$
S	Intervention indicator vector	F, f_k	SEM functions
$X_{\mathcal{I}}$	Set of intervened nodes	id	Identity map
$X_{\mathcal{O}}$	Set of non-intervened nodes	$(\text{id} - F)$	Function mapping X to ϵ
$p_\epsilon(\epsilon)$	Exogenous noise density function	$J_{\text{F}}(X)$	Jacobian matrix of F at X
$p_X(X), p(X, R)$	Target, full laws	$\mathbf{I}$	$K \times K$ Identity matrix
$p(Y\|X, R)$	Coarsening mechanism	$\mathbf{D}$	Matrix of intervention masks
$p(R\|X)$	Missingness mechanism	$\boldsymbol{B}$	Weighted adjacency matrix of linear SEM
$p(\boldsymbol{M}\|\theta)$	Gumbel-Softmax distribution for sampling $\boldsymbol{M}$	$\boldsymbol{M}$	Dependency mask for SEM function F
$\Theta = (\theta, \phi)$	Parameters of $p_X(X)$, $p(R\|X)$	$\boldsymbol{\Lambda}$	Inverse covariance matrix
Θ^t	Parameters at EM t-th iteration	$\mathbf{D}_i$	Intervention mask corresponding to i-th sample
Γ, Ω	Index sets for observed, missing nodes	i	Sample index variable
w_k, z_k	Parameters of $p(R_k \mid \text{pa}_{\mathcal{G}_m}(R_k))$	n	Total sample size
$(y^{(i)}, r^{(i)}, s^{(i)})$	i-th sample	n_B	Mini batch size in each EM
$\boldsymbol{A} \odot \boldsymbol{B}$	Hadamard product of $\boldsymbol{A}$ and $\boldsymbol{B}$	m	Power series expansion index for log-determinant of Jacobian
$\|\cdot\|_1$	L1 norm	N	Number of power series terms
$q(\cdot)$	Proposal distribution for rejection sampling	W	Gaussian random variable used for computing trace of Jacobian
$\mathcal{R}(\cdot)$	Sparsity inducing regularizer	$e^{\boldsymbol{A}}$	Matrix exponent of $\boldsymbol{A}$
$h_1(\phi)$	No colluders constrain function	$h_2(\phi)$	DAG constraint function

B Theory

B.1 Joint Density of Variables X: Target Law

Consider the structural equation model $X = \mathrm{F}(X)+\epsilon$, which implies $X = (\mathrm{id}-\mathrm{F})^{-1}(\epsilon)$. Using the properties of probability density functions, the joint distribution of $X = (X_1, \ldots, X_K)$ is given by,

$$p_X(X) = p_\epsilon\big((\mathrm{id}-\mathrm{F})(X)\big)\Big|\det J_{(\mathrm{id}-\mathrm{F})}(X)\Big|, \tag{23}$$

where $p_\epsilon(\epsilon)$ is the probability density function of the exogenous noise vector ϵ. Under an interventional setting $(X_\mathcal{I}, X_\mathcal{O})$, all incoming edges to the nodes in $X_\mathcal{I}$ are removed, leading to the following structural equations:

$$X_k = \begin{cases} \tilde{X}_k & \text{if } X_k \in X_\mathcal{I} \\ f_k\big(\mathrm{pa}_\mathcal{G}(X_k)\big) & \text{if } X_k \notin X_\mathcal{I} \end{cases}$$

That is, X_k is set to a known value $\tilde{X}_k$ if it is intervened upon, and the structural equation remains unchanged when X_k is purely observed. The above equation can be written more concisely as follows:

$$X_k = d_k \cdot \Big(f_k(\mathrm{pa}_\mathcal{G}(X_k)) + \epsilon_k\Big) + C_k, \quad \text{for } k = 1, \ldots, K. \tag{24}$$

where $d_k = \mathbb{1}\{X_k \notin X_\mathcal{I}\}$, and $\mathbb{1}\{\cdot\}$ is the indicator function, and $C_k = \tilde{X}_k$ if $X_k \in X_\mathcal{I}$, and $C_k = 0$ otherwise. Let $\mathbf{D} \in \mathbb{R}^{K\times K}$ be a diagonal matrix such that $D_{kk} = d_k$. Thus, equation 24 can now be combined for $k = 1, \ldots, K$ to obtain the following equation,

$$X = \mathbf{D}\mathrm{F}(X) + \mathbf{D}\epsilon + C, \tag{25}$$

where $F(X)$ is defined in Section 2 and $C = (C_1, \ldots, C_K)$. Thus we have, $(\mathrm{id} - \mathbf{D}\mathrm{F})(X) = \mathbf{D}\epsilon + C$, this implies that $X = (\mathrm{id} - \mathbf{D}\mathrm{F})^{-1}(\mathbf{D}\epsilon + C)$. Let $X_\mathcal{I} \sim p_{X_\mathcal{I}}(X_\mathcal{I})$. By the probability rules, we can write equation 23 as:

$$p_X(X) = p_{X_\mathcal{I}}(X_\mathcal{I})\; p_{\epsilon_\mathcal{O}}(\epsilon_\mathcal{O})\; \Big|\det J_{(\mathrm{id}-\mathbf{D}\mathrm{F})}(X)\Big|, \tag{26}$$

where $\epsilon_\mathcal{O}$ is the exogenous noise terms of variables in $X_\mathcal{O}$.

B.2 Convergence Analysis

Here we provide the convergence analysis of MissNODAG. Our analysis relies on the convergence of the EM algorithm (Wu, 1983; Friedman, 1998). The crux of the analysis depends on establishing that the total log-likelihood of the non-missing nodes in the data set either increases or stays the same in each iteration of the algorithm. That is,

$$\sum_{i=1}^{n} \log p\big(x^{(i)}_{\Gamma_i}, r^{(i)}|\Theta^{t+1}\big) \geq \sum_{i=1}^{n} \log p\big(x^{(i)}_{\Gamma_i}, r^{(i)}|\Theta^{t}\big). \tag{27}$$

To that end, note that

$$\sum_{i=1}^{n} \log p(x^{(i)}_{\Gamma_i}, r^{(i)}|\Theta) = \sum_{i=1}^{n} \log p(x^{(i)}_{\Gamma_i} x^{(i)}_{\Omega_i}, r^{(i)}|\Theta) - \sum_{i=1}^{n} \log p(x^{(i)}_{\Omega_i}|x^{(i)}_{\Gamma_i}, r^{(i)}, \Theta).$$

Taking expectation with respect $x^{(i)}_{\Omega_i}|x^{(i)}_{\Gamma_i}, r^{(i)}$ on both side, we get

$$\begin{aligned}\sum_{i=1}^{n} \log p(x^{(i)}_{\Gamma_i}, r^{(i)}|\Theta) &= \sum_{i=1}^{n} \mathbb{E}_{x^{(i)}_{\Omega_i}|x^{(i)}_{\Gamma_i}, r^{(i)}, \Theta^t} \log p(x^{(i)}_{\Gamma_i}, r^{(i)}|\Theta) \\ &= \underbrace{\sum_{i=1}^{n} \mathbb{E}_{x^{(i)}_{\Omega_i}|x^{(i)}_{\Gamma_i}; \Theta^t} \log p(x^{(i)}_{\Gamma_i} x^{(i)}_{\Omega_i}, r^{(i)}|\Theta)}_{=Q(\Theta|\Theta^t)} - \sum_{i=1}^{n} \mathbb{E}_{x^{(i)}_{\Omega_i}|x^{(i)}_{\Gamma_i}; \Theta^t} \log p(x^{(i)}_{\Omega_i}|x^{(i)}_{\Gamma_i}, r^{(i)}, \Theta).\end{aligned} \tag{28}$$

The first term on the RHS in the above equation is nothing but $Q(\Theta|\Theta^t)$. This is maximized in the M-step, i.e., $Q(\Theta|\Theta^{t+1}) \geq Q(\Theta|\Theta^t)$. On the other hand,

$$\sum_{i=1}^{n} \mathbb{E}_{x_{\Omega_i}^{(i)}|x_{\Gamma_i}^{(i)},r^{(i)};\Theta^t} \log \frac{p(x_{\Omega_i}^{(i)}|x_{\Gamma_i}^{(i)}, r^{(i)}, \Theta^{t+1})}{p(x_{\Omega_i}^{(i)}|x_{\Gamma_i}^{(i)}, r^{(i)}, \Theta^{t})} = -D_{KL}\Big(p(x_{\Omega_i}^{(i)}|x_{\Gamma_i}^{(i)}, r^{(i)}, \Theta^t)\big\|p(x_{\Omega_i}^{(i)}|x_{\Gamma_i}^{(i)}, r^{(i)}, \Theta^{t+1})\Big) \leq 0.$$

Thus,

$$\sum_{i=1}^{n} \mathbb{E}_{x_{\Omega_i}^{(i)}|x_{\Gamma_i}^{(i)},r^{(i)};\Theta^t} \log p(x_{\Omega_i}^{(i)}|x_{\Gamma_i}^{(i)}, r^{(i)}, \Theta^{t+1}) \leq \sum_{i=1}^{n} \mathbb{E}_{x_{\Omega_i}^{(i)}|x_{\Gamma_i}^{(i)},r^{(i)};\Theta^t} \log p(x_{\Omega_i}^{(i)}|x_{\Gamma_i}^{(i)}, r^{(i)}, \Theta^{t}). \tag{29}$$

From combining equation 28 and equation 29, we can see that at the end of the M-step equation 27 is satisfied. Similar to the previous results on EM convergence (Wu, 1983; Friedman, 1998), MissNODAG reaches a stationary point of the optimization objective.

B.3 Consistency of MissNODAG

In this subsection we establish the theoretical foundations for proving consistency of exact maximization of the MissNODAG score function. We begin by reviewing the relevant definition and prior results necessary to prove Theorem 2.

B.3.1 Background

Consider a directed graph $\mathcal{G} = (X, \mathcal{E})$. A *path* π between nodes X_i and X_k is a sequence $(X_{i_0}, X_{i_1}, \ldots, X_{i_n})$, with $X_{i_0} = X_i$, $X_{i_n} = X_k$, and every two consecutive nodes in the sequence are connected by an edge, i.e., either $X_{i_j} \to X_{i_{j+1}} \in \mathcal{E}$ or $X_{i_j} \leftarrow X_{i_{j+1}} \in \mathcal{E}$ for all $j = 0, \ldots, n-1$, with X. A path is *directed* if all the edges from X_i to X_k are oriented the same way. A cycle through node X_i consists of a directed path from X_i to a node X_j and the directed edge $X_j \to X_i$. For a node X_i, the set of *ancestors* is defined as $\text{an}_{\mathcal{G}}(X_i) := \{X_j \in X \mid \text{a directed path exists between } X_j \text{ and } X_i\}$. Similarly, the *descendant* of a node is defined as $\text{de}_{\mathcal{G}}(X_i) := \{X_j \in X \mid \text{a directed path exists between } X_i \text{ and } X_j\}$. The *strongly connected component* of a node X_i is given by the intersection of the ancestors and the descendants of X_i, i.e., $\text{sc}_{\mathcal{G}}(X_i) = \text{an}_{\mathcal{G}}(X_i) \cap \text{de}_{\mathcal{G}}(X_i)$. We can apply these definitions to subsets $X_{\mathcal{U}}$ by taking the union over all the elements in the subset, i.e., $\text{de}_{\mathcal{G}}(X_{\mathcal{U}}) = \cup_{i \in \mathcal{U}} \text{de}_{\mathcal{G}}(X_i)$. Finally, a node X_i is called a *collider* in a path π if it satisfies the following two conditions: (i) it is a non-endpoint node, and (ii) the subpath (X_k, X_i, X_j) is of the form $X_k \to X_i \leftarrow X_j$.

In an acyclic graph, the notion of d-separation is used to relate structural properties in the graph $\mathcal{G}$ to independencies in generated distribution. This is known as the *directed global Markov property* Forré & Mooij (2017). However, in general, cyclic graphs do not obey this property and a generalization of d-separation in the form of σ-separation was proposed by Forré & Mooij (2017) to characterize the relationship between graphical properties in a cyclic graph to the independencies observed in the distribution.

Definition B.1 (σ-separation)**.** *Let $\mathcal{G} = (X, \mathcal{E})$ be a directe graph and let $X_C \subseteq X$ be a subset of nodes. A path $\pi = (X_{i_0}, X_{i_1}, \ldots, X_{i_n})$ is said to be σ-blocked given X_C if*

1. *the first node of π, $X_{i_0} \in X_C$ or its last node $X_{i_n} \in X_C$, or*
2. *π contains a collider $X_j \notin X_C$,*
3. *π contains a non-collider $X_j \in X_C$ that points towards a neighbor that is not in the same strongly connected component as X_j in $\mathcal{G}$, i.e., $X_k \leftarrow X_j \in \pi$ and $X_k \notin sc_{\mathcal{G}}(X_j)$, or $X_j \to X_\ell \in \pi$ and $X_\ell \notin sc_{\mathcal{G}}(X_j)$.*

The path π is said to be σ-open given X_C if it is not σ-blocked. Two subsets of nodes $X_A, X_B \subseteq X$ is said to be σ-separated given X_C if all the paths between X_a and X_b, where $a \in A$ and $b \in B$, are σ-blocked given X_C, and is denoted by

$$X_A \overset{\sigma}{\underset{\mathcal{G}}{\perp\!\!\!\perp}} X_B \mid X_C.$$

σ-separation defined above reduces to d-separation in acyclic graphs. We can now define the generalized version of directed global Markov property for cyclic graphs.

Definition B.2 (General directed global Markov property Forré & Mooij (2017))**.** *Let $\mathcal{G} = (X, \mathcal{E})$ be a directed graph and p denote the probability density of the observations X. The probability density p satisfies the* general directed global Markov property *if for $X_A, X_B, X_C \subseteq X$*

$$X_A \overset{\sigma}{\underset{\mathcal{G}}{\perp}} X_B \mid X_C \implies X_A \underset{p}{\perp} X_B \mid X_C,$$

where $X_A \perp_p X_B \mid X_C$, denotes conditionally independence of X_A and X_B given X_C with respect to p.

Note that all the statements made above doesn't exactly depend on the vertex set. Thus, we can replace $\mathcal{G}$ with the m-graph $\mathcal{G}_m$ and retain all the properties stated earlier on the new graph with the vertex set (X, R).

B.3.2 Joint Causal Modeling of Interventions

To unify multiple interventional settings, we adopt the *joint causal model* Mooij et al. (2020). We create a *meta system* by augmenting the system variables (X, R) with exogenous context variables $C^{\mathcal{I}} = (C_1, \ldots, C_M)$, where each C_m corresponds to a specific intervention target set $X_{\mathcal{I}_m}$ and $C_m = \emptyset$ for all $m = 1, \ldots, M$ denotes the observational setting. We construct an augmented graph $\mathcal{G}_m^{\mathcal{I}}$ where the children of each context variable are its targets ($\mathrm{ch}_{\mathcal{G}}(C_m) = X_{\mathcal{I}_m}$). Given these targets and context variables, the structural equations for X take the form:

$$\tilde{f}_k(\mathrm{pa}^{\mathcal{I}}_{\mathcal{G}_m}(X_k), \epsilon_k) = \begin{cases} (C_m)_k, & \text{if } X_k \in I_m, \\ f_k(\mathrm{pa}_{\mathcal{G}}(X_k)) + \epsilon_k, & \text{if } X_k \notin I_m. \end{cases}$$

Note that $\mathrm{pa}^{\mathcal{I}}_{\mathcal{G}_m}(X_k)$ includes nodes from both X and $C^{\mathcal{I}}$. We call the distribution over the context variables $p(C^{\mathcal{I}})$ the *context distributions* and as noted by Mooij et al. (2020). We assume access to the context distribution as the interventional settings are known apriori. Note that, the observational distribution corresponds to $p_{\mathcal{G}^{\mathcal{I}}}(X \mid C_1 = \cdots = C_M = \emptyset)$. Similarly, the interventional distribution for the interventional targets $X_{\mathcal{I}_m}$ corresponds to $p_{\mathcal{G}^{\mathcal{I}}}(X \mid C_m = \boldsymbol{\xi}_{\mathcal{I}_m}, C_{-m} = \emptyset)$, i.e.,

$$p_{\mathcal{G}^{\mathcal{I}}}(X \mid C_m = \boldsymbol{\xi}_{\mathcal{I}_m}, C_{-m} = \emptyset) = p_{\mathrm{do}(\mathcal{I}_m)(\mathcal{G}_m)}(X).$$

Here, $p_{\mathrm{do}(\mathcal{I}_m)(\mathcal{G}_m)}$ corresponds to the interventional distribution generated by $\mathcal{G}_m$ for the interventional setting $X_{\mathcal{I}_m}$. Furthermore,

$$p_{\mathcal{G}^{\mathcal{I}}}(C^{\mathcal{I}}, X) = p_{\mathcal{G}^{\mathcal{I}}}(C^{\mathcal{I}}) p_{\mathcal{G}^{\mathcal{I}}}(X \mid C^{\mathcal{I}}). \tag{30}$$

Note that the missingness mechanism is unaltered by augmented the graph with context variables. Thus,

$$p_{\mathcal{G}^{\mathcal{I}}_m}(X, R, C^{\mathcal{I}}) = p_{\mathcal{G}^{\mathcal{I}}_m}(C^{\mathcal{I}}) p_{\mathcal{G}^{\mathcal{I}}_m}(X \mid C^{\mathcal{I}}) p_{\mathcal{G}_m}(R \mid X). \tag{31}$$

Recall, for the interventional setting $X_{\mathcal{I}_m}$, the probability density function governing the observations X is given by equation 4, which we repeat here for convenience

$$p_{\mathrm{do}(\mathcal{I}_m)(\mathcal{G})}(X) = p_I(X_I) p_\epsilon(\epsilon_{\mathcal{O}}) \left| \det \left(J_{(\mathrm{id} - \mathbf{DF})}(X) \right) \right|,$$

Definition B.3. *Let $\mathcal{G} = (X, \mathcal{E})$ be a directed graph, and $\{X_{\mathcal{I}_m}\}_{m=0}^M$ with $X_{\mathcal{I}_0} = X$ be a family of interventional targets. Let $\mathcal{M}_{\mathcal{I}}(\mathcal{G}_m)$ denote the set of positive densities $p_{\mathcal{G}^{\mathcal{I}}_m} : \mathbb{R}^{3d} \to \mathbb{R}$ such that $p_{\mathcal{G}^{\mathcal{I}}_m}$ is given by equation 31 for all $\mathrm{F} : \mathbb{R}^d \to \mathbb{R}^d$, with $f_i(X) = f_i(pa_{\mathcal{G}}(X_i))$, such that the resulting forward map $(id - \mathrm{F})$ is invertible, for all $(\sigma_1^2, \ldots, \sigma_K^2)$ such that $\epsilon \sim \mathcal{N}(0, Diag(\sigma_1^2, \ldots, \sigma_K^2))$, and positive density $p_{\mathcal{G}^{\mathcal{I}}_m}(R \mid X) : \mathbb{R}^{2d} \to \mathbb{R}$.*

Proposition B.4. *Let $\mathcal{G} = (X, \mathcal{E})$ be a directed graph, and $\{X_{\mathcal{I}_m}\}_{m=0}^M$ with $X_{\mathcal{I}_0} = X$ be a family of interventional targets, let $p \in \mathcal{M}_{\mathcal{I}}(\mathcal{G}_m)$, then p satisfies the general directed global Markov property relative to $\mathcal{G}^{\mathcal{I}}_m$.*

Proof. For a directed graph $\mathcal{G}$ and a choice of $\mathrm{F} : \mathbb{R}^d \to \mathbb{R}^d$ such that $(\mathrm{id} - \mathrm{F})$ is invertible, the structural equations are uniquely solvable with respect to each strongly connected component of $\mathcal{G}$. Moreover, the addition of context variables and the missingness indicators in the augmented graph does not introduce any new cycles. Therefore the meta system forms a simple SCM. Thus, from Theorem A.21 in (Bongers et al., 2021), the distribution $p_{\mathcal{G}_m^{\mathcal{I}}}$ is unique and it satisfies the general directed global Markov property. □

We now define the notion of interventional Markov equivalence class for DMGs based on the set of distribution induced by them.

Definition B.5 ($\mathcal{I}$-Markov Equivalence Class)**.** *Two directed mixed graphs $\mathcal{G}_m$ and $\mathcal{G}'_m$ are $\mathcal{I}$-Markov equivalent if and only if $\mathcal{M}_{\mathcal{I}}(\mathcal{G}_m) = \mathcal{M}_{\mathcal{I}}(\mathcal{G}'_m)$, denoted as $\mathcal{G}_m \equiv_{\mathcal{I}} \mathcal{G}'_m$. The set of all directed mixed graphs that are $\mathcal{I}$-Markov equivalent to $\mathcal{G}_m$ is the $\mathcal{I}$-Markov equivalence class of $\mathcal{G}_m$, denoted as $\mathcal{I}$-MEC$(\mathcal{G}_m)$.*

B.3.3 Proof of Theorem 2

We now present the main result of this paper. Recall the score function introduced in Section 3.1,

$$\mathcal{S}(\mathcal{G}_m) := \sup_{\Theta_{\mathcal{G}_m}} \sum_{m=1}^{M} \mathbb{E}_{(X_\Gamma, R) \sim p_{\text{obs}}^{(m)}} \log p_{\text{do}(I_m)(\mathcal{G})}(X_\Gamma, R) - \lambda |\mathcal{G}_m|,$$

where $p_{\text{obs}}^{(m)}$ is the observed part of the data-generating distribution for $X_{\mathcal{I}_m} \in \{X_{\mathcal{I}_m}\}_{m=0}^{M}$, and $\Theta = (\theta_{\mathcal{G}_m}, \phi_{\mathcal{G}_m})$ represents the model parameters. In the context of the meta system, since we assume access to the context distribution, the score function above is equivalent to the following score:

$$\mathcal{S}_{\mathcal{I}}(\mathcal{G}_m) := \sup_{\Theta} \mathop{\mathbb{E}}_{(X_\Gamma, R, C) \sim p_{\mathcal{I}}^*} \log p_{\mathcal{G}_m^{\mathcal{I}}}(X_\Gamma, R, C \mid \Theta) - \lambda |\mathcal{G}_m|,$$

where $p_{\mathcal{G}_m^{\mathcal{I}}}(X, R, C \mid \Theta)$ is given by equation 31 for a specific choice of Θ, and $p_{\mathcal{G}_m^{\mathcal{I}}}(X_\Gamma, R, C \mid \Theta)$ corresponds to the restriction to only the observed nodes. $p_{\mathcal{I}}^*$ denotes the joint ground-truth distribution for the observed and the context variables. We define $\mathcal{P}_{\mathcal{I}}(\mathcal{G}_m)$ as the set of all distributions $p_{\mathcal{G}_m^{\mathcal{I}}}(X, R, C \mid \Theta)$ that can be expressed by the model specified by equation 3, equation 13, and equation 18. That is,

$$\mathcal{P}_{\mathcal{I}}(\mathcal{G}) := \{p \mid \exists\, \Theta \text{ s.t } p = p_{\mathcal{G}_m^{\mathcal{I}}}(\cdot \mid \Theta)\}. \tag{32}$$

From the above definition it is clear that $\mathcal{P}_{\mathcal{I}}(\mathcal{G}_m) \subseteq \mathcal{M}_{\mathcal{I}}(\mathcal{G}_m)$. Theorem 2 relies on the following set of assumptions. The first one ensures that the model is capable of representing the ground truth distribution.

Assumption B.6 (Sufficient Capacity)**.** *The joint ground truth distribution $p_{\mathcal{I}}^*$ is such that $p_{\mathcal{I}}^* \in \mathcal{P}_{\mathcal{I}}(\mathcal{G}_m^*)$, where $\mathcal{G}_m^*$ is the ground truth m-graph.*

In other words, there exists a Θ such that $p_{\mathcal{I}}^* = p_{\mathcal{G}_m^{\mathcal{I}}}(\cdot \mid \Theta)$. The second assumption generalizes the notion of faithfulness assumption to the interventional setting.

Assumption B.7 ($\mathcal{I}$-σ-faithfulness)**.** *Let $V = (X, R, C^{\mathcal{I}})$, for any subset of nodes $A, B, D \subseteq \mathcal{V} \cup C^{\mathcal{I}} \cup R$, and $I_m \in \mathcal{I}$*

$$A \underset{\mathcal{G}_m^{\mathcal{I}}}{\overset{\sigma}{\not\perp}} B \mid B \implies V_A \underset{p_{\mathcal{G}_m^{\mathcal{I}}}}{\not\perp} V_B \mid V_C.$$

The above assumption implies that any conditional independency observed in the data must imply a σ-separation in the corresponding interventional ground truth graph.

Assumption B.8 (Finite differential entropy)**.** *For a family of interventional targets $\{X_{\mathcal{I}_m}\}_{m=0}^{M}$,*

$$|\mathbb{E}_{p_{\mathcal{I}}^*} \log p_{\mathcal{I}}^*(X, C)| < \infty.$$

The above assumption ensures that the hypothetical scenario where $\mathcal{S}(\mathcal{G}^*)$ and $\mathcal{S}(\mathcal{G})$ are both infinity is avoided. This is formalized in the lemma below taken from (Brouillard et al., 2020).

Lemma B.9 (Finiteness of the score function (Brouillard et al., 2020))**.** *Under assumptions B.6 and B.8,* $|\mathcal{S}_{\mathcal{I}}(\mathcal{G})| < \infty$.

We finally make the assumption that the density are strictly positive.

Assumption B.10 (Strict positivity)**.** *For all* $V = (X, C, R)$, $p_{\mathcal{G}_m^{\mathcal{I}}}(V) > 0$ *for all* $p_{\mathcal{G}_m^{\mathcal{I}}} \in \mathcal{M}_{\mathcal{I}}(\mathcal{G}_m)$.

From the results of (Brouillard et al., 2020), we can now express the difference in score function between $\mathcal{G}_m^*$ and $\mathcal{G}_m$ as the minimization of KL diverengence plus the difference in the regularization terms.

Lemma B.11 (Rewritting the score function (Brouillard et al., 2020))**.** *Under assumptions B.6 and B.8, we have*

$$\mathcal{S}(\mathcal{G}_m^*) - \mathcal{S}(\mathcal{G}_m) = \inf_{\phi} D_{KL}(p^*_{\mathcal{I},obs} \| p_{\mathcal{G}_m^{\mathcal{I}},obs}(\cdot \mid \Theta)) + \lambda(|\mathcal{G}_m| - |\mathcal{G}_m^*|).$$

where $p_{\cdot,obs}(\cdot)$ *denotes the distribution restricted to only the observed variables.*

Furthermore, under complete data, Sethuraman & Fekri (2025) showed that the KL divergence appearing the in lemma above is strictly positive.

Lemma B.12 (Lemma A.18, Sethuraman & Fekri (2025))**.** *Let* $\mathcal{G} = (\mathcal{V}, \mathcal{E})$ *be a directed graph, for a set of interventional targets* $\{X_{\mathcal{I}_m}\}_{m=0}^M$, *and* $p^* \notin \mathcal{M}_{\mathcal{I}}(\mathcal{G}_m))$, *then*

$$\inf_{p \in \mathcal{M}_{\mathcal{I}}(\mathcal{G}_m))} D(p^* \| p) > 0.$$

We now extend this result to the case of missing data.

Lemma B.13. *Let* $\mathcal{G} = (\mathcal{V}, \mathcal{E})$ *be a directed graph, for a set of interventional targets* $\{X_{\mathcal{I}_m}\}_{m=0}^M$, *and* $p^* \notin \mathcal{M}_{\mathcal{I}}(\mathcal{G}_m))$, *then*

$$\inf_{p \in \mathcal{M}_{\mathcal{I}}(\mathcal{G}_m))} D(p^*_{obs} \| p_{obs}) > 0.$$

Proof. From Lemma B.12, we know that if $p^* \notin \mathcal{M}_{\mathcal{I}}(\mathcal{G}_m))$ then for the full distribution we have

$$\inf_{p \in \mathcal{M}_{\mathcal{I}}(\mathcal{G}_m))} D(p^* \| p) > 0.$$

This implies that p^* does not conform to the independencies enforced by the σ-separation constraints of $\mathcal{G}_m$. Let us now assume, for the sake of contradiction, that the infimum of the score on the observed data is zero:

$$\inf_{p \in \mathcal{M}_{\mathcal{I}}(\mathcal{G}_m))} D(p^*_{\text{obs}} \| p_{\text{obs}}) > 0.$$

By Pinsker's inequality, this implies convergence in total variation and thus convergence in distribution. Therefore, there exists a sequence of distributions $\{p^{(k)}_{\text{obs}}\}_{k=1}^{\infty} \subset \mathcal{M}_{obs}(\mathcal{G}_m)$ such that:

$$\lim_{k \to \infty} p^{(k)}_{\text{obs}} = p^*_{\text{obs}},$$

where $\mathcal{M}_{obs}(\mathcal{G}_m)$ denotes the projection of the distributions Markov to $\mathcal{G}_m$ restricted to just the observed variables.

Let Ψ be the identification mapping established by Nabi et al. (2020) such that $\Psi(p_{obs}) = p$. From Assumption 1 and Assumption B.10 the map Ψ is surjective, and since Ψ consists of elementary algebraic operations (marginals, multiplications, divisions), it is a continuous function with respect to the distribution. Applying the continuous map Ψ to the sequence:

$$\lim_{k \to \infty} \Psi(p^{(k)}_{\text{obs}}) = \Psi\Big(\lim_{k \to \infty} p^{(k)}_{\text{obs}}\Big) = \Psi(p^*_{\text{obs}}) = p^*.$$

Let $g^{(k)} = \Psi(p^{(k)}_{\text{obs}})$. Since $p^{(k)}_{\text{obs}}$ is generated by the model $\mathcal{G}_m$, its identified full law $g^{(k)}$ must be a valid distribution in the full model $\mathcal{M}(\mathcal{G}_m)$.

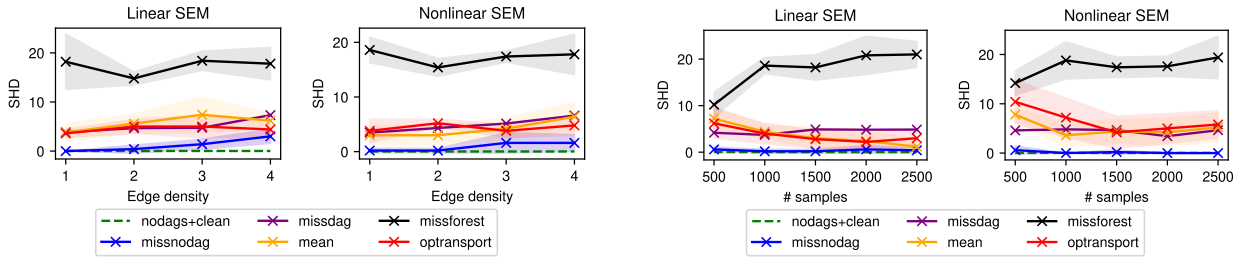

(a) Varying TL edge density

(b) Varying training samples

Figure 5: Target law recovery performance comparison on both linear and nonlinear SEM

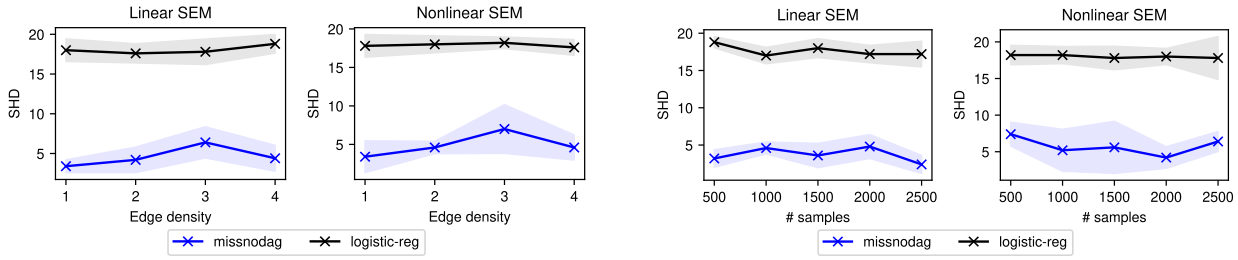

(a) Varying TL edge density

(b) Varying training samples

Figure 6: Missingness mechanism recovery performance comparison ($X \to R$ edges).

We now have a sequence $\{g^{(k)}\} \subset \mathcal{M}(\mathcal{G}_m)$ that converges to p^*. This would mean that

$$\inf_{p \in \mathcal{M}_{\mathcal{I}}(\mathcal{G}_m))} D(p^* \| p) = 0,$$

which is a contradiction. Therefore, the lemma holds. □

We are now ready to prove Theorem 2. Recall,

Theorem 2. *Let $\{X_{\mathcal{I}_m}\}_{m=0}^{M}$ be a family of interventional targets, let $\mathcal{G}_m^*$ denote the ground truth directed mixed graph, $p^{(k)}$ denote the data generating distribution for I_k, and $\hat{\mathcal{G}}_m := \arg\max_{\mathcal{G}_m \in \mathcal{G}_{id}} \mathcal{S}(\mathcal{G}_m)$. Then, under the Assumptions 1, B.6, B.7, B.8, and B.10, and for a suitably chosen $\lambda > 0$, we have that $\hat{\mathcal{G}}_m \equiv_{\mathcal{I}} \mathcal{G}_m^*$. That is, $\hat{\mathcal{G}}_m$ is $\mathcal{I}$-Markov equivalent to $\mathcal{G}_m^*$.*

Proof. The proof is a direct extension of Theorem 2 in Sethuraman & Fekri (2025), with Lemma B.13 substituting Lemma B.12.

□

C Additional Experiments

C.1 Sensitivity to Model Parameters

We conducted an sensitivity analysis comparing MissNODAG with baseline models to assess sensitivity to: (a) number of samples per intervention in the training set, and (b) average edge density of the target law graph. In all cases, graphs were generated using the ER random graph model. Training data consisted of single-node interventions over all nodes in the graph. Exogenous noise variables and m-graphs were sampled as described in Section 4. In all the cases we consider both the linear ($\beta = 0$) and the nonlinear SEM ($\beta = 1$). Results (averaged over 10 trials) are shown in Figures 5, 6, and 7.

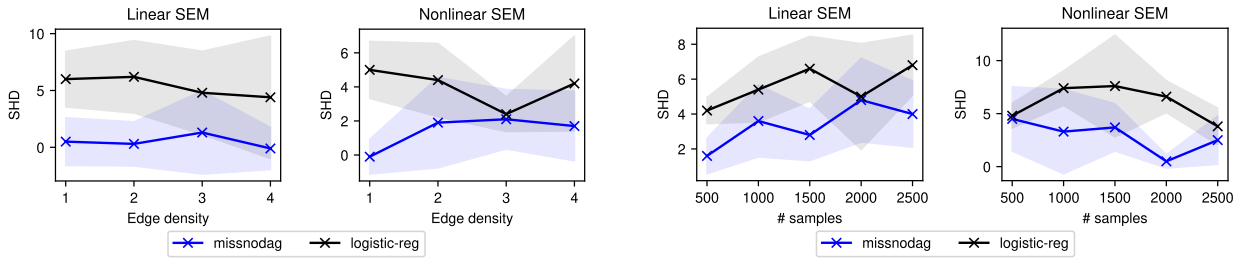

(a) Varying TL edge density

(b) Varying training samples

Figure 7: Missingness mechanism recovery performance comparison ($R \to R$ edges).

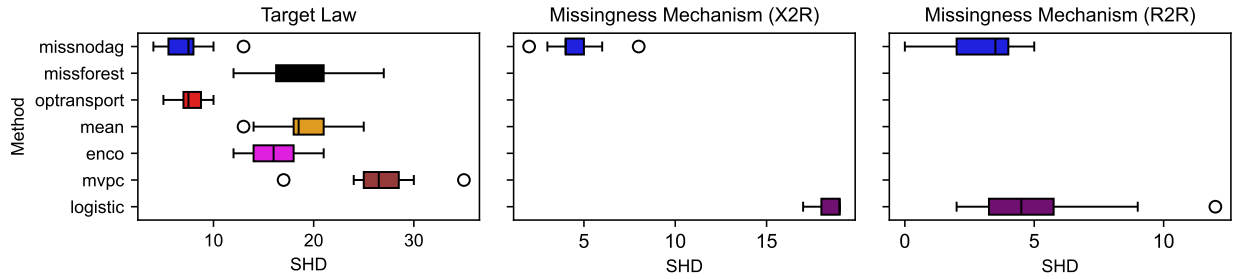

Figure 8: Performance comparison under soft interventions

Varying target law edge density. In our experiments, the outgoing edge density of the target law was varied between 1 and 4, while the average missing probability was fixed at 0.3 and the missingness mechanism edge density at 3. Each interventional setting comprised 1,000 samples. Overall, MissNODAG outperformed the baselines in recovering both the target law and the missingness mechanism. However, we observed that the models performed comparably in terms of target law and $R \to R$ edge recovery.

Varying interventional training samples. With the target law and missingness mechanism outgoing edge densities fixed at 2 and 3, respectively, we varied the number of training samples per interventional setting from 500 to 2,500 (in increments of 500). The average missingness probability was set to 0.3. The results exhibit a trend consistent with the previous experiment. Additionally, as the sample size increases, the performance gap between the methods narrows.

C.2 Misspecification

We consider three kinds of model misspecification: (i) soft interventions, (ii) non-identifiable missingness mechanism, and (iii) mismatched parametric family for missingness mechanism. In each setting, the we considered nonlinear SEM with $K = 10$ nodes, missing probability set to 0.3 and provided a single node interventions as training input.

Soft interventions. In this setting, the interventional structure equation model is set as follows:

$$X_k = \begin{cases} \tilde{f}_k\big(\mathrm{pa}_{\mathcal{G}}(X_k)\big) + \tilde{\epsilon}_k & \text{if } X_k \in X_{\mathcal{I}} \\ f_k\big(\mathrm{pa}_{\mathcal{G}}(X_k)\big) + \epsilon_k & \text{if } X_k \notin X_{\mathcal{I}} \end{cases}$$

In our case, we set $\tilde{f}_k = f_k$ and consider $\epsilon_k \sim \mathcal{N}(0, \sigma_k^2)$, $\tilde{\epsilon}_k \sim \mathcal{N}(\mu_k, \sigma_k^2)$, with $\mu_k = 1$ (also known as shift interventions). In this case, the parent-child interactions are preserved under intervention. The results are summarized in Figure 8. As seen from the figure, MissNODAG achieves comparable performance to that of the baselines, albeit achieving higher SHD score compared to hard interventions.

Non-identifiable missingness mechanism. Here, we explicitly add self-censoring edges as well as colluders into the missingness mechanism while considering hard interventions. The results are summarized in Figure 9. As seen from the figure, MissNODAG is still capable of learning the target law, however, the absolute SHD score increases for missingness mechanism recovery.

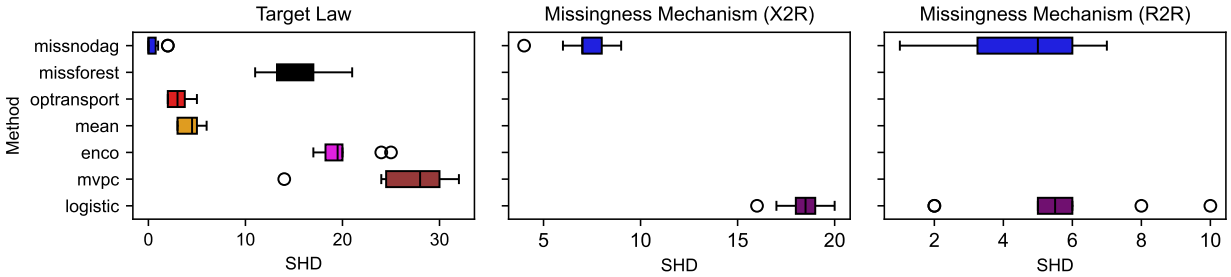

Figure 9: Performance comparison on non-identifiable missingness mechanism

Mismatched parametric family for missingness mechanism. In this setting, we consider the conditional distribution corresponding to each missingness mechanism R_i to be as follows:

$$p\big(R_k = 0 \mid \mathrm{pa}_{\mathcal{G}_m}(R_k), \phi_k\big) = \mathrm{expit}\big(NN_k(X, R) + z_k\big),$$

where $NN_k(X, R)$ is a 2-layer neural network with tanh activation. The results are summarized in Figure 10. As seen from the, the absolute SHD score for target law recovery has increased compared to the well-specified case, however, MissNODAG still retains a comparable performance to that of the baselines.

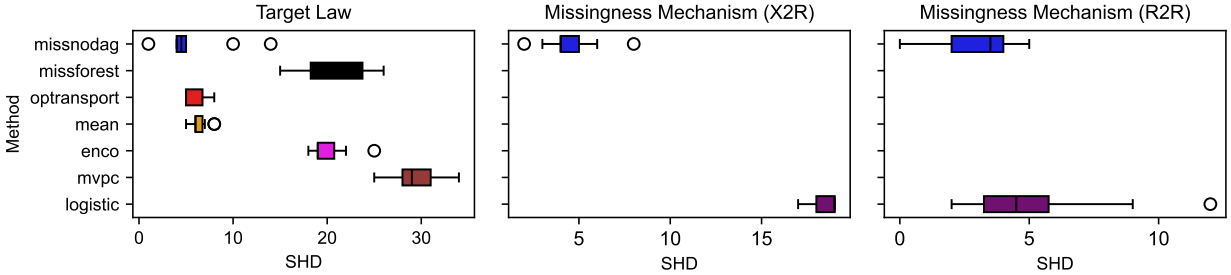

Figure 10: Performance comparison under missingness mechanism misspecification

C.3 Computation Time and Convergence Analysis

In Figure 11, we compare the training times of MissNODAG and the baselines for two settings: $K = 10$ nodes (left) and $K = 20$ nodes (right). In both cases, the training data consists of single-node interventions on all nodes, with 500 samples per intervention. MissNODAG and MissDAG were trained for 100 epochs. For other baselines, the reported time includes both data imputation and subsequent training of NODAGS-Flow on the imputed data for 100 epochs. We also report the training time of NODAGS-Flow itself. The two primary computational bottlenecks in MissNODAG are the rejection sampling procedure and the computation of the Jacobian log-determinant, which is required during both the imputation and target law update stages. Utilizing a power series approximation yields a complexity of $\mathcal{O}(K^2)$ for the log-determinant, which can be further reduced in practice via the Hutchinson trace estimator. Consequently, the overall time complexity of MissNODAG is $\mathcal{O}(K^2 L)$, where L denotes the maximum number of rejection sampling steps.

As shown in Figure 11, MissNODAG requires the longest training time, though only slightly more than MissDAG in both settings. This additional time is primarily due to jointly learning the missingness mechanism, which MissDAG does not model. As expected, compute time approximately doubles when the number of nodes is doubled.

Additionally, we report the training and eval metrics (log probability of observations, no colluder constraint function value, DAG constraint on $R \to R$ edges, and target law SHD) as a function training iterations in Figure 12.

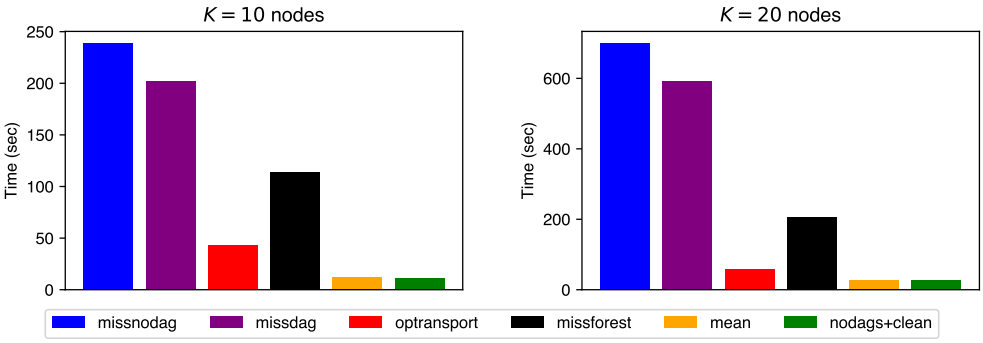

Figure 11: Training time comparison

C.4 Sachs Protein Signaling Dataset

We evaluate MissNODAG on a biological dataset for protein signaling network discovery Sachs et al. (2005), which is widely used as a benchmark for causal discovery algorithms.

The dataset contains continuous measurements of multiple phosphorylated proteins and phospholipid components in human immune system cells, with the corresponding network capturing the ordering of interactions among pathway components. Based on $n = 7466$ samples across $m = 11$ cell types, Sachs et al. (2005) identified 20 edges in the underlying graph. Using the consensus network from Sachs et al. (2005) as ground truth, we evaluate performance using the Structural Hamming Distance (SHD) as the error metric. Since the data doesn't contain any missing values, we define a synthetic missingness mechanism to generate missing data from the complete dataset. We set the missing probability to 0.3. The results are summarized in Table 3. From the table we can see that MissNODAG performs comparably to the baselines. The recovered directed graph is visualized in Figure 14.

Table 3: Performance comparison on Sachs et al. (2005) protein signaling dataset.

Method	**TL-SHD**
MissNODAG	**20**
MissDAG	23
Optransport + NODAGS	22
Optransport + ENCO	23

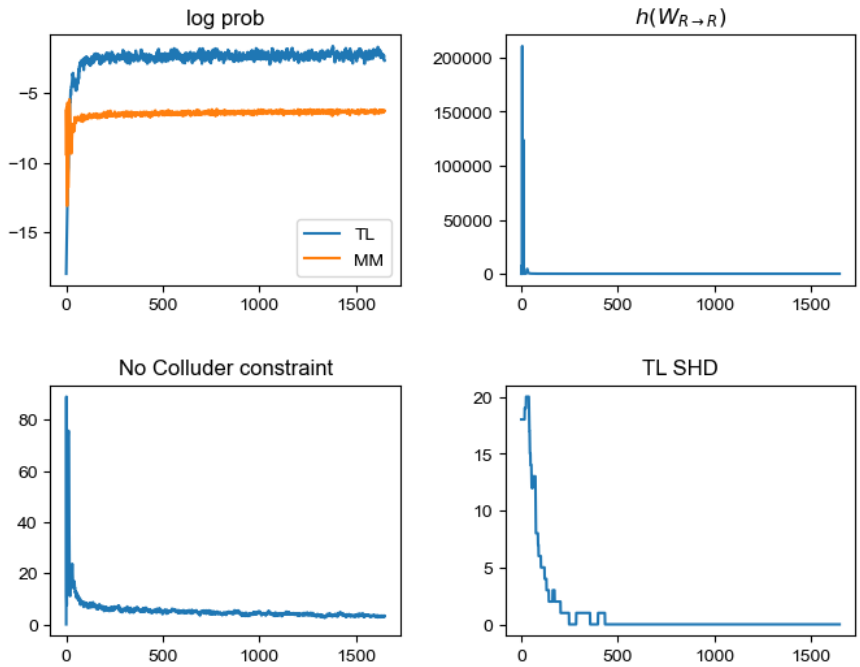

Figure 12: Training and evaluation metrics as a function of training iterations. Top left: log probability of the observed data for both target law and missingness mechanism. Top right: DAG constraint for $R \to R$ edges. Bottom left: no colluder constraint for missingness mechanism. Bottom right: target law SHD.

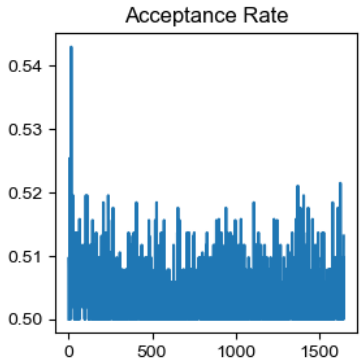

Figure 13: Rejection sampling acceptance rate during versus training iterations.

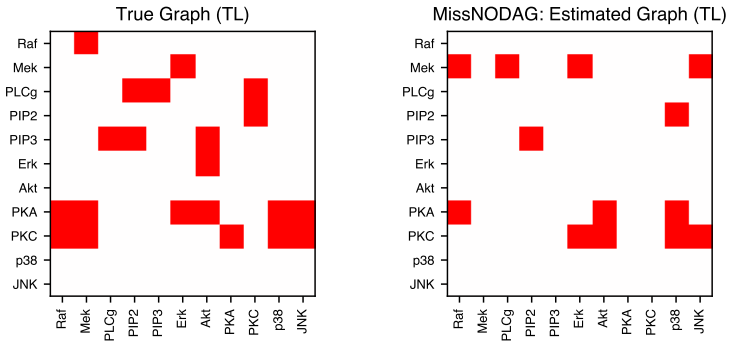

Figure 14: (Left) Consensus graph from Sachs et al. (2005), (right) graph learned by MissNODAG.

D Implementation Details

In this section, we describe the implementation details of the MissNODAG framework and the baseline models used for performance comparisons.

MissNODAG. We implemented our framework using the Pytorch library in Python and the code used in running the experiments can be found in the `codes` folder within the supplementary materials. We plan to make the code publicly available on GitHub upon publication of the paper.

Starting with an initialization of the model parameters Θ^0, we alternate between the E-step and M-step until the parameters converge. In the E-step, Algorithm 1 is used for imputing the missing data, followed by maximizing the expected likelihood of the non-missing nodes in the M-step. We follow the same setup as Sethuraman et al. (2023) for modeling the causal functions, i.e., neural networks (NN) along with dependency mask with entries parameterized by Gumbel-softmax distribution, and for computing the log-determinant of the Jacobian, i.e., power series expansion followed by Hutchinson trace estimator. Poisson distribution is used for $p_{\mathbb{N}}$ for sampling the number of terms in the expansion to reduce the bias introduced while limiting the number of terms in the power series expansion of log-determinant of the Jacobian, see section 3.3. The final objective in the M-step is maximized using Adam optimizer (Kingma & Ba, 2014).

The learning rate in all our experiments was set to 10^{-2}. The neural network models used in our experiments contained one multi-layer perceptron layer. No nonlinearities were added to the neural networks for the linear SEM experiments. We used tanh activation for the nonlinear SEM experiments and ReLU activation for the experiments on the perturb-CITE-seq data set. The regularization constant λ was set to 10^{-2} for the synthetic experiments and 10^{-3} for the perturb-CITE-seq experiments. All experiments were performed on NVIDIA RTX6000 GPUs.

Baselines. For the baseline NODAGS-Flow, we modify the code base provided by Sethuraman et al. (2023) to use the imputed samples for maximizing the likelihood. The hyperparameters of NODAGS-Flow was set to the values described in the previous subsection.

MissForest imputation is performed using the publicly available python library `missingpy`. We use the codebase provided by Muzellec et al. (2020) for optimal transport imputation, and the codebase provided by the authors was used for MissDAG (Gao et al., 2022). The default parameters are used for Missforest, optimal transport imputation, and MissDAG. The codes for all the baselines can be found inside the `codes` folder in the supplementary materials.